Journal of Computational Physics **151,** 358–387 (1999)
Article ID jcph.1999.6222, available online at http://www.idealibrary.com on IDEAL®

# Molecular Dynamics Simulation of Membranes and a Transmembrane Helix

Tap Ha Duong, Ernest L. Mehler, and Harel Weinstein[1]

*Department of Physiology and Biophysics, Mount Sinai School of Medicine, New York, New York 10029*
E-mail: hweinstein@inka.mssm.edu

Received October 9, 1998; revised February 8, 1999

Three molecular dynamics (MD) simulations of 1.5-ns length were carried out on fully hydrated patches of dimyristoyl phosphatidylcholine (DMPC) bilayers in the liquid-crystalline phase. The simulations were performed using different ensembles and electrostatic conditions: a microcanonical ensemble or constant pressure-temperature ensemble, with or without truncated electrostatic interactions. Calculated properties of the membrane patches from the three different protocols were compared to available data from experiments. These data include the resulting overall geometrical dimensions, the order characteristics of the lipid hydrocarbon chains, as well as various measures of the conformations of the polar head groups. The comparisons indicate that the simulation carried out within the microcanonical ensemble with truncated electrostatic interactions yielded results closest to the experimental data, provided that the initial equilibration phase preceding the production run was sufficiently long. The effects of embedding a non-ideal helical protein domain in the membrane patch were studied with the same MD protocols. This simulation was carried out for 2.5 ns. The protein domain corresponds to the seventh transmembrane segment (TMS7) of the human serotonin $5HT_{2A}$ receptor. The peptide is composed of two $\alpha$-helical segments linked by a hinge domain around a perturbing Asn-Pro motif that produces at the end of the simulation a kink angle of nearly $80^\circ$ between the two helices. Several aspects of the TMS7 structure, such as the bending angle, backbone $\Phi$ and $\Psi$ torsion angles, the intramolecular hydrogen bonds, and the overall conformation, were found to be very similar to those determined by NMR for the corresponding transmembrane segment of the tachykinin NK-1 receptor. In general, the simulations were found to yield structural and dynamic characteristics that are in good agreement with experiment. These findings support the application of simulation methods to the study of the complex biomolecular systems at the membrane interface of cells. 

[1] To whom correspondence should be addressed.



0021-9991/99 $30.00

## INTRODUCTION

The stability, high resolution structure and dynamics of protein $\alpha$-helices have been the focus of many studies addressing both the folding process and the biological functionality of these basic secondary structure units. These studies are especially relevant for gaining insights into the relationships between structure and function of many transmembrane (TM) proteins, such as ion channels or G protein coupled receptors (GPCR). The membrane spanning portions of these proteins are often constituted of $\alpha$-helix bundles. For this reason, the characterization of the interactions between such molecular assemblies and their membrane environments present a special interest [1–4]. Moreover, the proposed role of the membrane bilayer in modulating TM protein structure [5, 6] makes it essential to understand the mutual effects and dynamics of single $\alpha$-helices embedded in an explicit membrane bilayer environment.

Both pure membrane and membrane-peptide complex structures have been studied and characterized by different experimental approaches. These have yielded valuable information about average values of properties that are important in determining the dynamics and the structural details of the systems. Among the methods used to study lipid bilayer structure, infra-red (IR) spectroscopy provides information about the *trans* to *gauche* ratio in the hydrocarbon chains [7, 8], while x-ray and neutron diffraction methods provide information about the spatial distribution of the different groups of atoms relative to the membrane plane normal [9–11]. Nuclear magnetic resonance (NMR) has been used to characterize the internal conformations and dynamic behavior of the head groups and the acyl chains of lipid molecules [12–15], as well as the secondary structures and orientations of peptides embedded in bilayers [16–19]. The orientations of the acyl chains were probed in circular dichroism (CD) experiments [20, 21] or IR spectroscopy [22, 23]. Specific loci in bilayer-spanning helical polypeptides have been examined with time resolved fluorescence anisotropy (FA) measurements [24], or solid state NMR [25] which revealed the dynamic behavior of tryptophan residues relative to the membrane. Similarly, details about lipid-peptide interactions have emerged from NMR spectroscopy and from differential scanning calorimetry (DSC) IR, and x-ray studies [26–30].

In spite of the tantalizing insights provided by these initial studies of very complex systems, many of the observations remain poorly understood at the atomic level. Complementary insights about these biologically important membrane-protein systems have emerged from computational approaches. For example, Monte Carlo (MC) simulations have been used to study the dependence of lipid-protein interactions on the form and size of the protein (e.g., see [31]), and to describe thermodynamic properties of membrane-protein complexes in terms of heat capacity profiles and protein distribution [32]. Using both on-lattice and off-lattice Monte Carlo simulation, Skolnick and Milik have captured the essence of the physical basis for spontaneous insertion of several peptides into implicit lipid membrane [33].

In parallel, molecular dynamics (MD) simulations with a great variety of conditions and parametrizations are increasingly utilized to gain insights into the structure and dynamics of both pure membrane patches membrane-peptide complexes [4, 34–48]. To improve the utility, reliability, and economy of such simulations, much attention has been devoted to searching for the optimal conditions of simulations that best fit the experiments on pure membrane systems. These include boundary conditions imposing constant volume, ensemble definitions such as constant pressure or constant surface tension, the treatment of electrostatic interactions with a cutoff distance, Ewald summation, or others methods.

However, a unique protocol has not emerged that systematically succeeds in reproducing the experimental observations.

Recently, several MD simulations of polypeptides surrounded by a lipid bilayer have been published. Despite the significant computational cost of such simulations, some of them have included entire transmembrane proteins, including Bacteriorhodopsin [49], Gramicidin A Channel [50], the Pf1 Coat Protein [51], a 5-HT2A receptor model [52], and the OmpF Porin [53]. Some studies have focused on the stability, structure, and dynamics of isolated $\alpha$-helix immersed in a membrane bilayer that explored the role of the hydrophilic and hydrophobic domains of the membrane in stabilizing protein secondary structure. Yet other studies have probed how phospholipids restrict the peptide internal flexibility or how a polypeptide insertion affects the surrounding lipid molecules [3, 54–59].

Here we report on MD simulations of dimyristoyl phosphatidylcholine (DMPC) bilayers containing the putative transmembrane segment 7 (TMS7) of the serotonin $5HT_{2A}$ human receptor, a member of the G protein coupled receptor (GPCR) family. The structural and dynamics properties of this segment are of special interest since they are believed to have an important role in the signal transduction function of GPCRs through conformational changes induced by agonist binding [60, 61]. In particular, TMS7 contains an absolutely conserved proline residue, which has been implicated in the functionally important kinking of the helix [62], and in flexibility properties related to the proline kink [63–69]. The purpose of this study is to understand how the bilayer membrane can stabilize, by interplaying between intra- and inter-molecular interactions, the TMS7 structure in which some backbone hydrogen bonds are broken because of the proline residue positioned around its middle. Moreover, we have investigated the restrictions imposed by the phospholipid membrane on the structure of the isolated TMS7 and the effects of the polypeptide on the physical properties of the surrounding membrane.

The simulation of the peptide-containing membrane patch follows a protocol defined from a comparison of results from the three different simulations of the pure DMPC bilayer structures to experimental results. The first calculation (NVE-CUT) was performed in the microcanonical (NVE) ensemble, i.e., constant particle number, volume, and total energy, with electrostatic interactions truncated to a cutoff distance of 12 Å. The second protocol (NPT-CUT) was done in the NPT ensemble using the same truncation of the electrostatic interactions. The third simulation (NPT-EXT) was carried out in the NPT ensemble, but with long-range Coulomb interactions accounted for with the extended electrostatic method developed by Karplus and collaborators [70]. *Because the aim was to enable a direct comparison of the results of the three different lipid bilayers simulations with experimentally measured properties, the pure membrane systems were constructed to model at the atomic level of resolution samples used for NMR experiments.*

## METHODOLOGY

### *Initial Structures*

The nomenclature of the DMPC molecule is reported in Fig. 1 [71]. The initial coordinates of TMS7 used in the simulation of the peptide-containing membrane patch (protocol NVE-CUT-TMS7) were taken from a model proposed for this TM helix exhibiting the conserved NP/DP motif in the GPCR family [72]. This starting structure of the transmembrane segment is primarily in $\alpha$-helical form except at the position preceding the proline

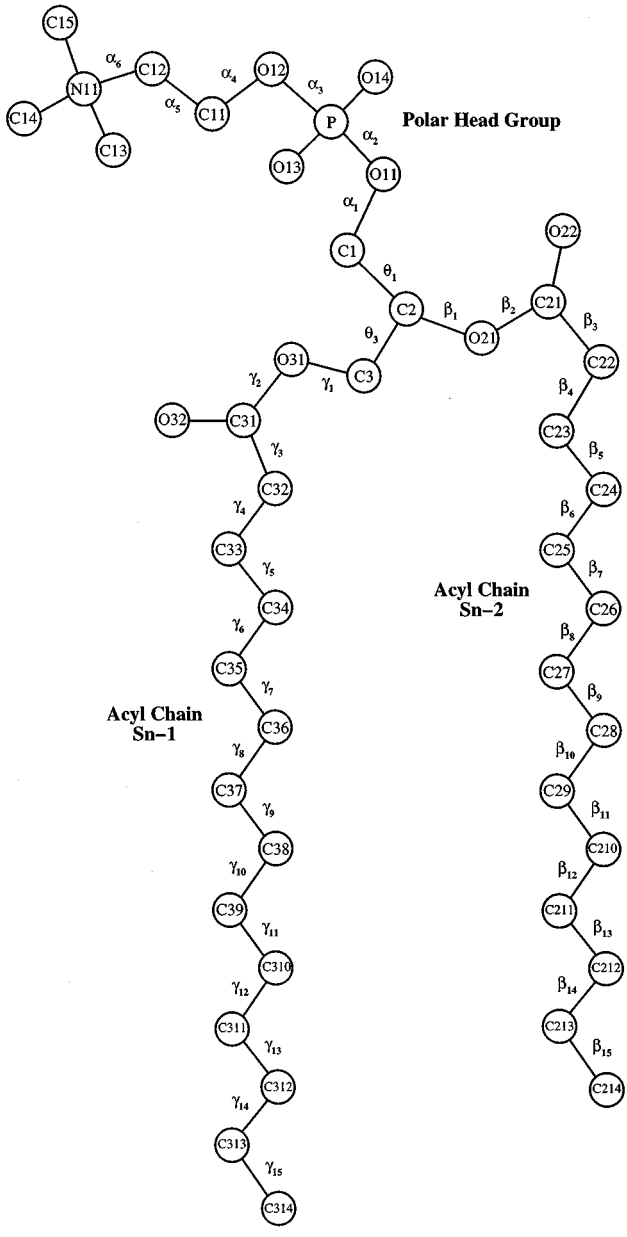


**FIG. 1.** Nomenclature of the DMPC molecule atoms and torsion angles [71].

that confers a bend of about 45° to the peptide [72]. The peptide consists of the sequence *ng*-LNVFVWIGYLSSAVNPLVYTLFN-*ng* where both ends have been capped with neutral groups (*ng*).

The two simulations identified above as NVE-CUT and NVE-CUT-TMS7 were carried out in the NVE ensemble with hexagonal periodic boundary conditions in the $XY$ direction. For the two constant pressure calculations, NPT-CUT and NPT-EXT, tetragonal boundary conditions were used. For all four simulations, the multilayer systems were constructed in the $Z$ direction using a periodic box length of 72 Å. The DMPC molecules (Fig. 1) were

assumed to have a cross sectional area of 64 Å$^2$, which represents an average value from experimental data [73–77]. The calculated cross sectional area of NVE-CUT-TMS7 varied from 100 Å$^2$ (at the termini) to 200 Å$^2$ (near the NP motif). A value of 180 Å$^2$ was used to construct the initial membrane-peptide complex. These parameters, combined with the requirement that a minimum of three lipids separate peptides in neighboring images, yielded a primary cell with an edge length of 24.7 Å and containing 22 lipids surrounding the helix in each leaflet . For the NVE-CUT simulation of the pure membrane patch, a primary cell with an edge length of 24.8 Å was built using 25 lipids in each leaflet, whereas an initial tetragonal box with an edge length of 41 Å and containing 26 lipids in each leaflet was constructed for both NPT simulations.

The construction of the initial hydrated lipid bilayers was carried out using a protocol developed by Benoit Roux and collaborators [50, 78] and briefly described below. The lipids were assembled into the primary cells (and around the peptide, when appropriate) by first placing spheres of 64 Å$^2$ cross sectional area (spherical pseudo-headgroups representing the molecular fragments) at random positions in *XY* planes situated at $Z = \pm 17$ Å. The assembly of pseudo-headgroups was subsequently energy minimized and subjected to MD simulations to relieve any close contacts. The coordinates of these spherical groups provide the sites for initial positioning of the explicit phospholipid headgroups. The DMPC molecules were randomly selected from a library of 2000 preequilibrated and prehydrated conformers. These had been generated from Monte Carlo simulations on isolated molecules, using a mean field approximation that was empirically adjusted to reproduce experimental data such as $^2$H quadrupolar splitting and $^{13}$C NMR relaxation time [47]. This procedure in the protocol from the Roux lab had been developed to reduce the long equilibration times that are required when MD simulations start from bilayer crystalline structures or for membrane-peptide patches built by deleting lipids from a pure bilayer state [79]. Optimal lateral packing is achieved by eliminating as many bad contacts as possible using a series of rigid body translations in the *XY* planes and rotations about the *Z* axis. Hydration was completed subsequently by immersing the membrane systems in water layers of about 15 Å thickness. Finally, the systems were further optimized to eliminate bad contacts using energy minimization and constrained Langevin dynamics simulations, as originally described by [47, 50, 78].

### *Simulation Details*

The CHARMM program package [80] was used for all MD simulations with the PAR22 all-atom force field including parameters for phospholipids [81] and the TIP3 water potential [82]. Electrostatic and Van der Waals group-based interactions were truncated at a cutoff distance of 12 Å with a smooth switching function over a 3 Å interval. A cutoff distance of 13 Å was used to calculate the nonbonded lists that were updated every five steps. The lengths of all bonds involving hydrogen atoms were constrained using the SHAKE algorithm [83] which allows a 2-fs time step to be used for the numerical integration of the equations of motion. For the two NPT simulations, the constant pressure is controlled by the Langevin piston method [84] derived from the extended system formalism [85]. The mass of the pressure piston and the Langevin piston collision frequency were respectively set to 250 A.M.U. and 25 ps$^{-1}$. The reference internal isotropic pressure of the simulated systems was equal to 1 Atm. In addition, the temperature control algorithm developed by Nose [87] and Hoover [86] was used with a mass of the thermal piston set to 500 Kcal.ps$^2$.

**TABLE I**
**Summary of the Four MD Simulations[a]**

| | Number of amino acids | Number of DMPC | Number of waters | Simulation length (ps) | Last velocity scaling (ps) |
|---|---|---|---|---|---|
| NVE-CUT | — | 50 | 2033 | 1550 | 325 |
| NPT-CUT | — | 52 | 1996 | 1730 | — |
| NPT-EXT | — | 52 | 1996 | 1600 | — |
| NVE-CUT-TMS7 | 25 | 44 | 1986 | 2525 | 670 |

[a] All calculations were performed at 37°C.

In all simulations, the reference temperature was set to 37°C (310°K) which is 13°C above the pure DMPC gel/liquid crystal transition temperature [88].

For each of the four simulations (NVE-CUT, NPT-CUT, NPT-EXT, and NVE-CUT-TMS7), a total of 180–200 ps of Langevin dynamics were run for equilibration while gradually decreasing the harmonic constraints imposed during the construction of the initial structures [50]. After this initial equilibration phase all constraints were relaxed and the systems allowed to evolve 1.5 ns for the pure membranes and around 2.5 ns for the membrane-peptide complex. (The time origin was fixed just after the Langevin dynamics phase.) After all constraints were relaxed, temperature scaling was allowed for an additional 50 ps for the two simulations in the NVE ensemble, and then the runs were continued in the production mode. We found, however, that this length of equilibration time was insufficient as evidenced by an increase in temperature starting after the first 100–200 ps of MD production. The protocol was therefore altered by allowing velocity scaling if the average temperature went out of a temperature window of $310 \pm 3$°K. Additional temperature scalings were observed for both simulations much later in the run, but after the last scaling (see Table I) the systems remained in equilibrium as shown by the complete constancy of the total energy and temperature (Fig. 2), allowing statistically valid data to be collected for one or more nanoseconds. Coordinates and energy data were saved every 0.2 ps and time averaged structural analyses were carried out using the last 500 ps of the trajectories for both pure membranes and the lipid-peptide complex. A summary of the four MD simulation parameters for all four systems is reported in Table I.

## RESULTS AND DISCUSSION

### *Structure Analysis of the Pure Membrane Patch*

*General aspects.* The evolution of the internal energy and lipid surface area of the three lipid bilayers is displayed in Fig. 2. From the energy plots, it can be seen that the NVE-CUT simulation seems to be well equilibrated after 325 ps of dynamics, but that the two NPT runs do not seem to achieve convergence until at least 700 ps. It should be noted that compared to the NPT-CUT calculation, the fluctuations of the internal energy in the NPT-EXT simulation remain large until about 1100 ps of simulation. Nevertheless, the trajectory for the last 500 ps appears to be quite stable (no significant drifting) and was therefore used for all analyses. About 600 ps into the trajectory, the lipid surface areas of the two constant pressure simulations reached plateaus with values of 60 and 61 Å$^2$ for NPT-CUT and NPT-EXT, respectively. These are somewhat lower than the lipid surface

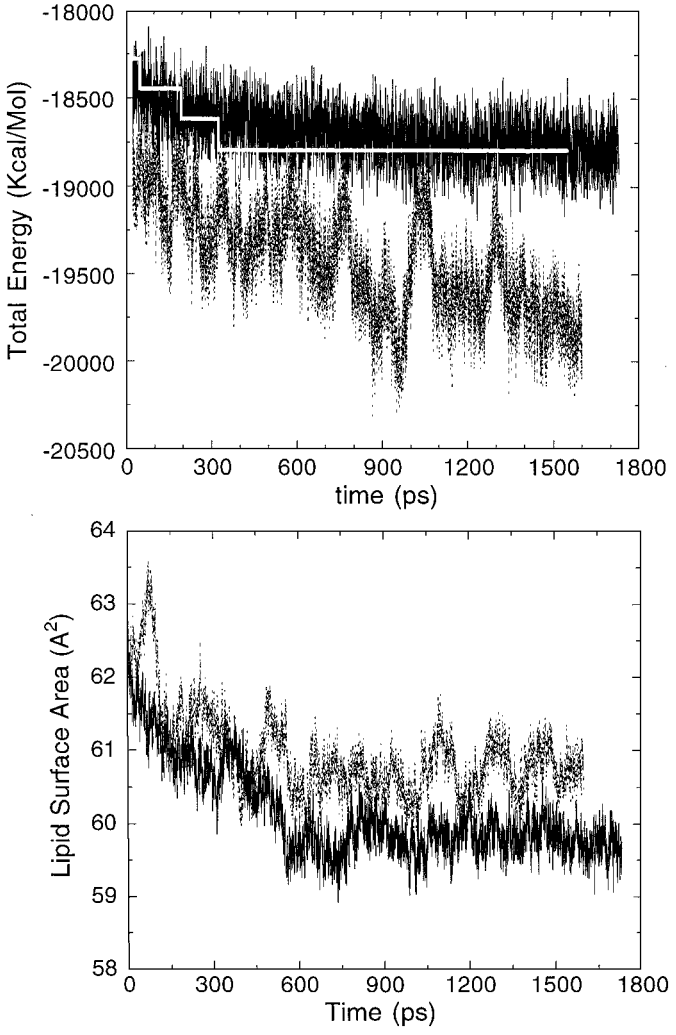


**FIG. 2.** Time evolution of the total energy (upper panel) and the lipid surface area (lower panel) for the pure membrane simulations NVE-CUT (light line), NPT-CUT (solid line), and NPT-EXT (dashed line).

area of 64 $Å^2$ assigned initially (Fig. 2), but all these values of the DMPC surface area are in the range of experimental measurements (59–70 $Å^2$) [73–77]. As reported in Table II, the computed volume per lipid and bilayer thickness are in relatively good agreement with experimental measurements, with errors less than 5% [74, 76, 77, 89]. The thickness of the hydrophobic region for the two NPT simulations is larger than the experimental estimation by around 3 Å [76, 77], corresponding to an error of 12% (Table II). In terms of bilayer and hydrophobic region thickness, the NVE-CUT simulation gives better results than the two constant pressure calculations.

The average value of the membrane electron density profile along the bilayer normal was calculated from the last 500 ps of the trajectory. Comparison (Fig. 3) of the simulated electron density profiles with the profile measured by small-angle x-ray diffraction [9] shows that the positions and heights of the two peaks (corresponding to the lipid polar groups) in the MD profiles are quite similar and agree well with experiment. However, the calculated

**TABLE II**
**Comparison of Geometrical Parameters for Bilayers from Experiment and Simulation**

| | Surface area ($Å^2$) | Volume[a] ($Å^3$) | Bilayer thickness[b] (Å) | Hydrophobic thickness[c] (Å) | Percentage of *gauche* bonds |
|---|---|---|---|---|---|
| NVE-CUT | 63.9 | 1081 | 35.3 | 24.6 | 18 |
| NPT-CUT | 59.8 | 1061 | 36.5 | 25.9 | 17 |
| NPT-EXT | 60.8 | 1095 | 36.0 | 25.8 | 19 |
| Nagle *et al.* [10] | — | 1109 (37) | — | — | — |
| Janiak *et al.* [74] | 62.2 (37) | — | 35.5 (37) | — | — |
| Lewis *et al.* [76] | 65.7 (36) | — | 34.0 (36) | 23.0 (36) | — |
| De Young *et al.* [79] | 70.0 (35) | — | — | — | — |
| Rand *et al.* [77] | 65.0 (27) | — | 34.5 (27) | 22.3 (27) | — |
| Koenig *et al.* [75] | 59.5 (30) | — | — | — | — |
| Casal *et al.* [7] | — | — | — | — | 25 (29) |
| Pink *et al.* [91] | — | — | — | — | 27 (30) |
| NVE-CUT-TMS7 | 64.1 | — | 35.7 | 25.0 | 18 |

[a] Calculated from the relation $V_{box} = N_{lip}V_{lip} + N_{wat}V_{wat}$ where $V_{box}$, $N_{lip}$, and $N_{wat}$ are respectively the volume of the cell and the number of lipid and water molecules. $V_{lip}$ is the lipid volume and $V_{wat}$ is the volume per water molecule (30 $Å^3$).

[b] Computed as the difference between the average $Z$ coordinate of the phosphate and nitrogen atoms in the two leaflets of the bilayer.

[c] Calculated as the difference between the average $Z$ coordinate of the C22 and C32 atoms of the two leaflets of the bilayer. For experimental results, the measured temperature (in °C) is given in parentheses.

electron density profiles in the central region of the bilayer have minima that are too shallow with values around 0.25 e/$Å^3$ compared to the experimental value of about 0.17 e/$Å^3$. To a lesser extent, this phenomenon was also observed from molecular dynamics simulations of DPPC in the NPT ensemble [44, 46]. Because the position of the polar groups is in relatively

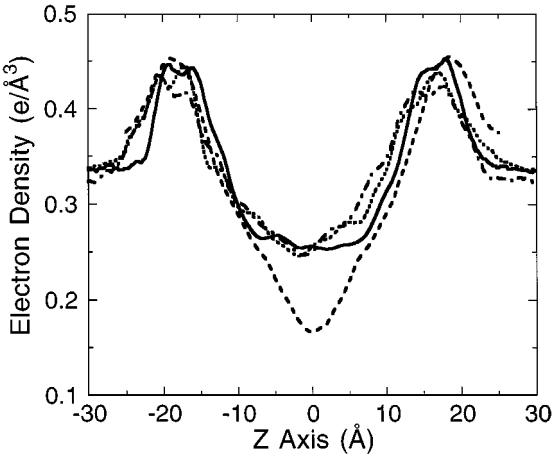


**FIG. 3.** Electron density profile along the bilayer normal for the pure membrane simulations, NVE-CUT (solid line), NPT-CUT (dotted line), and NPT-EXT (dotted-dashed line). The dashed curve is the profile resulted from x-ray diffraction study at 35°C [9].

good agreement with experiment, such shallow minima in the middle of the bilayer suggest that these MD simulations overestimate the orientational order of the lipid acyl chains. The simulated system seems to be closer to the gel state than suggested by the simulation temperature of 310°K. This would occur if the gel-liquid crystal transition temperature of the DMPC bilayer in the CHARMM22 force field were inappropriately higher than the experimental transition temperature of 298°K.

*Acyl chain conformation.* The liquid crystal state of the membrane's hydrocarbon chain region can be characterized by two different physical quantities: the number of *gauche* C–C bonds and the deuterium order parameters of C–D bonds in the lipid acyl chains. In contrast to a membrane bilayer in the crystalline state where all the acyl chain C–C bonds are in the *trans* conformation [90], the hydrocarbon chains of DMPC bilayers in the fluid phase have an average percentage of *gauche* C–C bonds of about 25–27% as measured by Raman and infra-red spectroscopies at 30°C [7, 91]. In the simulations, the percentage of lipid acyl chain C–C bonds in the *gauche* conformation (averaged over the last 500 ps) is about 18% which is lower than the experimental estimates by about one bond per acyl chain (Table II).

In a complementary way, the deuterium order parameter, $S_{C-D}$, provides an estimate of the motional anisotropy of the deuterated C–D bonds in the lipid acyl chain: If $\Theta$ denotes the angle between a C–D bond and the bilayer normal, then the order parameter is given by

$$S_{C-D} = (1/2)\langle 3\mathrm{Cos}^2(\Theta) - 1\rangle \tag{1}$$

(where the brackets $\langle\ \rangle$ indicate a time average) and can be measured directly from the NMR deuterium quadrupole splitting,

$$\Delta\nu_Q = (3/4)(e^2qQ/h)|S_{C-D}|, \tag{2}$$

where the constant $e^2qQ/h$ is equal to 170 KHz for aliphatic C–D bonds [15]. Figure 4 presents the C–D deuterium quadrupole splitting $\Delta\nu_Q$ at several hydrocarbon positions of the DMPC acyl chain as calculated from MD simulations and as measured by NMR at 30°C [13]. The calculated order parameters were all found to be negative indicating that the highest values of $\Delta\nu_Q$ correspond to C–D bonds preferentially oriented in directions more parallel to the membrane plane. It can be observed that MD-calculated deuterium quadrupole splitting values are slightly higher than the experimental ones, indicating that the modeled acyl chains are overall more parallel to the bilayer normal than estimated from NMR.

The comparison with experiment of the number of C–C *gauche* bonds and order parameters of the C–D bond vectors within the membrane hydrocarbon region suggests that the *lipid acyl chains in the simulations are oriented too parallel to the membrane normal and are more ordered than they should be in the liquid crystal state*. Because the calculated bilayer thickness (or the averaged distance between phosphatidylcholine groups of the two layers) is close to the value observed experimentally (Table II), these structural features of the modeled hydrocarbon chains could lead to an excessive interpenetration of some lipid acyl chains into the opposite monolayer. This explains the shallow minimum observed in the calculated electron density profiles (Fig. 3). In spite of these small differences, the patterns exhibited by the calculated deuterium order parameter along the hydrocarbon chains are quite similar to those determined by NMR, showing that MD simulations can qualitatively

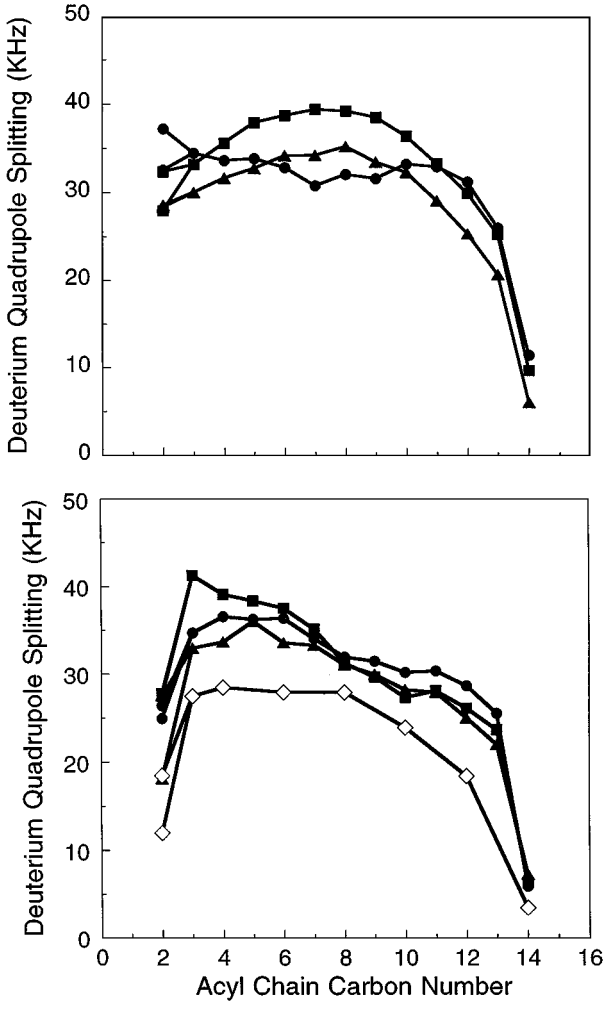


**FIG. 4.** Deuterium quadrupole splitting at different hydrocarbon positions on the DMPC acyl chains Sn-1 (upper panel) and Sn-2 (lower panel) calculated from the NVE-CUT (circle), NPT-CUT (square), and NPT-EXT (triangle) simulations and as measured by NMR study (diamond) at 30°C [13].

reproduce the disordered conformations of the acyl chains characteristic of the liquid crystal state.

*Polar group conformation.* The geometries of the lipid head groups calculated from the simulations are in quite good agreement with many NMR spectroscopy studies, despite some discrepancies in the internal conformational details. Consistent with neutron diffraction and NMR observations on phosphatidylcholine bilayers [92, 93], the averaged orientation of the DMPC head groups was found to be parallel to the membrane surface for the three MD calculations (Table III). The orientations of the lipid glycerol segments relative to the bilayer normal are also given in Table III as estimated by MD and NMR studies. It is seen that the calculated orientation of the C2–C1 bond, which constitutes the junction between the phosphatidylcholine group and the two hydrocarbon chains, is in good agreement with NMR results [94], whereas the calculated orientation of the C2–HC2 bond appears to be more parallel to the membrane surface than observed experimentally [95].

**TABLE III**
**Time Averaged Angle (in Degrees) between Different Lipid Headgroup Vectors and the Bilayer Normal**

| | P–N | C2–C1 | C2–C3 | C2–O21 | C2–HC2 | C1–P |
|---|---|---|---|---|---|---|
| NVE-CUT | 88 | 40 | 74 | 60 | 93 | 44 |
| NPT-CUT | 90 | 40 | 78 | 58 | 88 | 44 |
| NPT-EXT | 98 | 42 | 74 | 63 | 90 | 54 |
| Durfourc *et al.* [94] | — | 36 | — | — | — | — |
| Hong *et al.* [95] | — | 35 | — | — | 109 | — |
| NVE-CUT-TMS7 | 90 | 42 | 71 | 60 | 95 | 44 |

*Note*. Available NMR results are also reported for comparison.

Information on the spatial orientation of the lipid polar groups can be obtained from various NMR data [96, 97] including $^{13}C$–$^{1}H$ or $^{31}P$–$^{13}C$ dipolar coupling measurements [14, 95]. The $^{31}P$–$^{13}C$ dipolar couplings $\Delta\nu_D$ for ten carbon atoms of the head groups have been evaluated from the three MD simulations using the expression

$$\Delta\nu_D = 12236.5|\langle(3\mathrm{Cos}^2(\Theta) - 1)/(2R^3)\rangle|, \tag{3}$$

where $\Theta$ measures the angle between the C–P vectors and the bilayer normal and $R$ denotes the internuclear distances between the lipid phosphorus and the carbon atoms [14]. The results, given in Fig. 5, show that the NVE-CUT and NPT-CUT simulations qualitatively reproduce the measured P–C dipolar couplings for most of the carbon atoms, despite some slight discrepancies for the C11, C1, or C2 carbons [14]. In contrast, the dipolar coupling from the NPT-EXT simulation strongly disagrees with the measured value at carbon atom C1. For all three MD simulations the P–C dipolar couplings for C2, C21, and C22 carbons are lower than observed experimentally. According to the analysis of the NMR data given by Hong and co-workers [95], this suggests that the calculations underestimate the

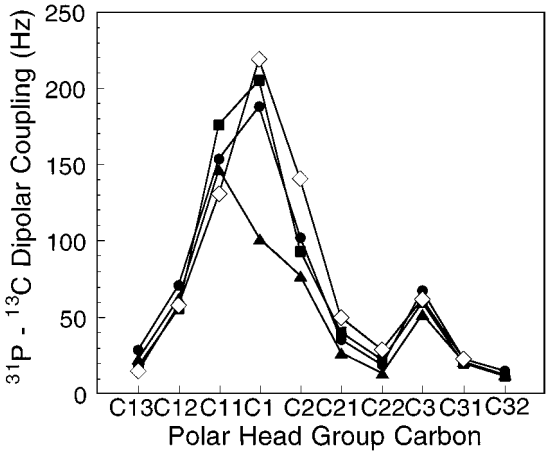


**FIG. 5.** $^{31}P$–$^{13}C$ dipolar coupling for ten carbon atoms of the DMPC headgroup calculated from the NVE-CUT (circle), NPT-CUT (square), and NPT-EXT (triangle) simulations and as measured from NMR (diamond) at 40°C [14].

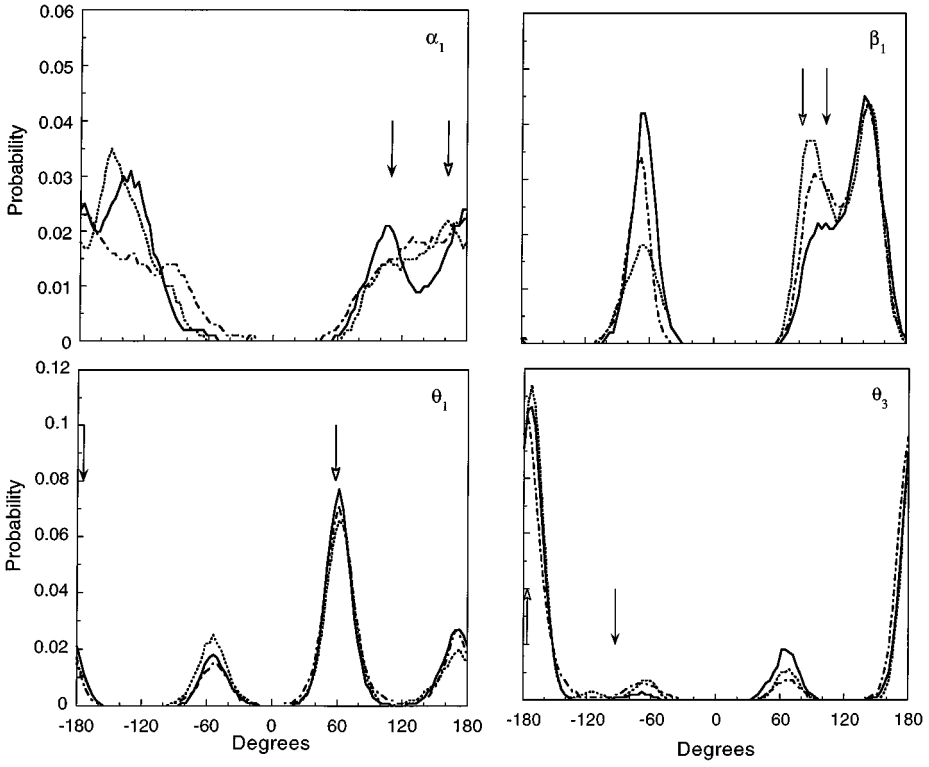


**FIG. 6.** Dihedral angles $\alpha_1$, $\beta_1$, $\theta_1$, and $\theta_3$ conformations in the DMPC headgroups calculated from the NVE-CUT (solid line), NPT-CUT (dotted line), and NPT-EXT (dotted-dashed line) simulations. Closed and opened arrows show experimental conclusions from Hong *et al.* [95] and Hauser *et al.* [96], respectively.

population of DMPC lipids in a conformation close to the crystalline molecule B, which is mainly characterized by a bend of the headgroup toward the Sn-2 acyl chain, and a *trans* configuration of the $\theta_1$ dihedral angle [90, 95] (see below).

Indeed, from the dihedral angles determining the conformation of DMPC headgroups (Fig. 6), it can be seen that the three MD simulations yield a majority of DMPC headgroups with the $\theta_1$ dihedral angle in *gauche+* conformation (the percentage of $\theta_1$ angle in *gauche+* conformation being 61, 58, and 65% whereas the percentage of *trans* conformation is 24, 20, and 21% for the NVE-CUT, NPT-CUT, and NPT-EXT simulations, respectively). In contrast, the dihedrals $\alpha_1$ and $\theta_3$ are principally in a *trans* conformation, whereas $\beta_1$ seems more variable (Fig. 6). Note that, in the *trans* region, the $\alpha_1$ angle distribution in the NPT-EXT simulation is slightly different from the two other calculations. This results in an averaged orientation of the P–C1 vector that is more perpendicular to the bilayer normal (Table III) and could explain the abnormally low P–C1 dipolar coupling in the NPT-EXT simulation (Fig. 5). These calculated preferential geometries differ significantly from the conclusions of Hong and co-workers ($\theta_1 = 185^\circ$, $\alpha_1 = 110^\circ$, $\theta_3 = -95^\circ$, $\beta_1 = 145^\circ$) and confer to most of the DMPC molecules a conformation in which the phosphatidylcholine groups tend to point toward the opposite direction of the Sn-2 chains, in a similar way as in the crystalline DMPC molecule A ($\theta_1 = 58^\circ$, $\alpha_1 = 163^\circ$, $\theta_3 = -178^\circ$, $\beta_1 = 82^\circ$) [96]. This result could explain the relatively low P–C dipolar couplings for the C2, C21, and C22 carbons in the MD simulations compared to NMR $^{31}$P–$^{13}$C dipolar coupling measurements.

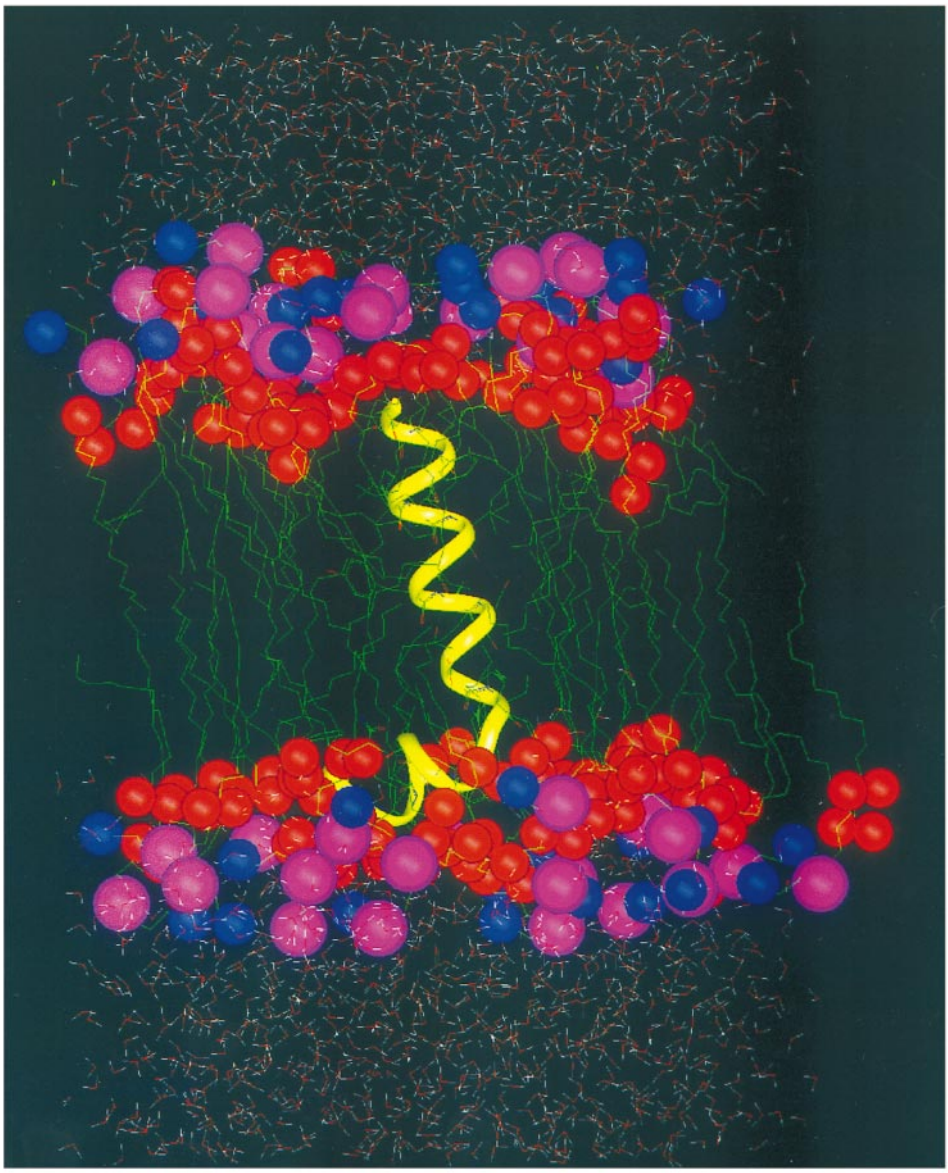

**FIG. 7.** Complete structure of the membrane-TMS7 complex embedded in water at the end of the NVE-CUT-TMS7 simulation. The view shows the extracellular region at the top of the figure. Shown in the CPK representation, the lipid headgroup phosphates (purple), the nitrogen atoms (blue), and the lipid glycerol oxygen atoms (red).

Nevertheless, it should be noted that in the NVE-CUT and NVE-CUT simulations the results of headgroup conformations may constitute only a slight deviation from experiment, since the precise proportions of lipids similar to the molecules A and B within a fluid membrane is still debated [94–97].

*Conclusion.* The analysis of the three separate 1.5-ns MD simulations of DMPC bilayers using different ensembles and electrostatic parameters indicates that the simulations yielded reasonable qualitative pictures of hydrated phospholipid membranes. The

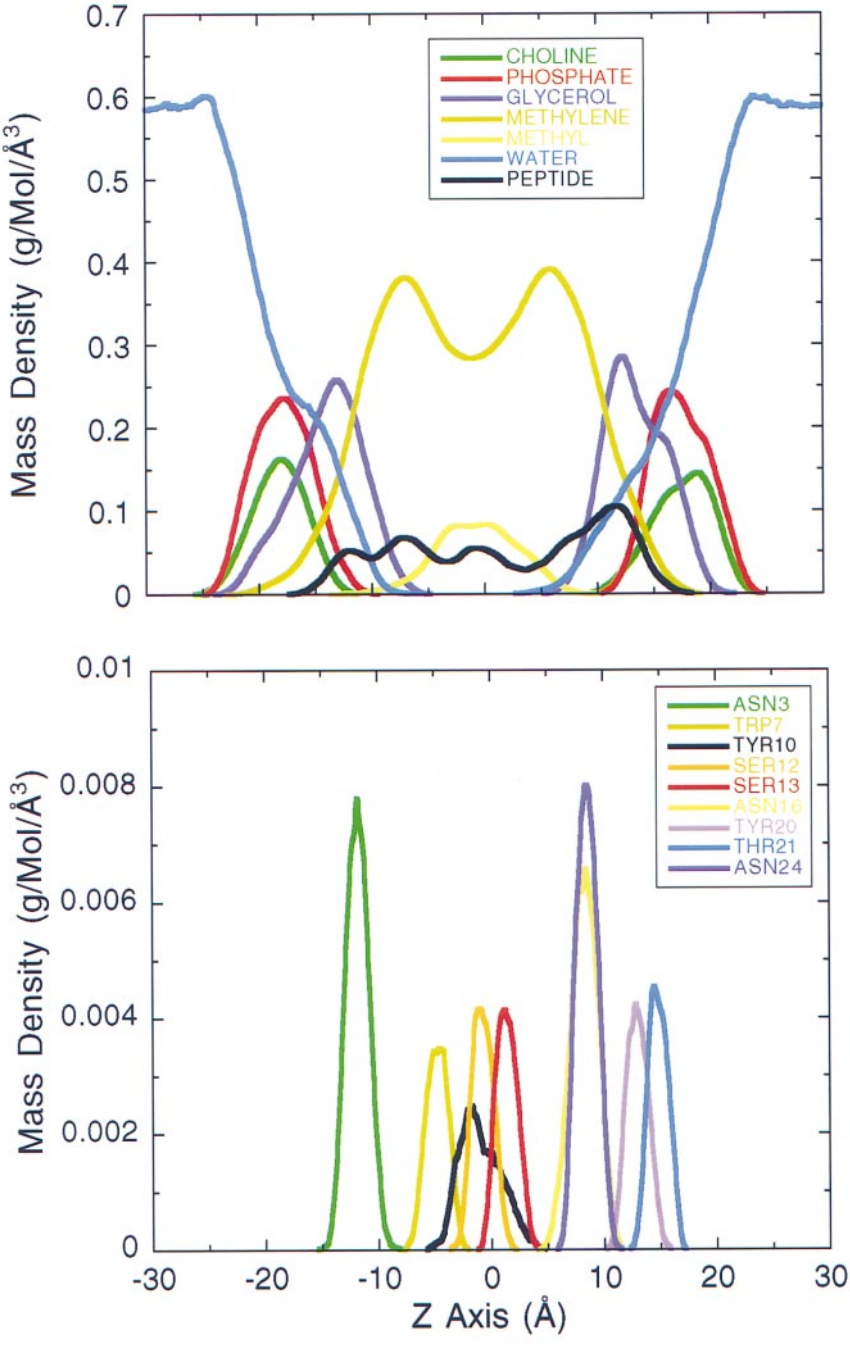


**FIG. 8.** Mass density profile along the bilayer normal (*Z* axis) for the different atomic groups of the membrane-peptide complex of TMS7 (upper panel), and of the polar side chain hydrogen bond donors and acceptors (lower panel).

calculated structural features are in reasonable general agreement with available experimental data, but some differences are evident in the details, including the percentage of the acyl chain C–C bond in the *gauche* configuration, and the predominant internal conformation of the polar headgroups. Such differences between calculated and experimental inferences about the orientation of the headgroups have also been observed in other MD simulations [36, 42, 43, 46]. From NMR studies the characteristic times of dihedral angle dynamic *trans-gauche* isomerizations within lipid molecules have been estimated to be in the range of 10–100 ps for the hydrocarbon chain C–C bonds [98] and in the range of 400–700 ps for the headgroup torsion angles [94]. Consequently, while it is likely that the discrepancies between MD simulations and experimental results are the result of inadequacies in the force field, the dynamics of the headgroup torsion angles is such that longer simulation times are indicated to explore the agreement with experiment [42, 43].

*Structure Analysis of the Membrane-Peptide Complex*

*General aspects.* Figure 7 shows a ribbon representation of the TMS7 peptide embedded in the membrane at the end of the NVE-CUT-TMS7 simulation. The $\alpha$-helical segment of the starting structure of the peptide is conserved, but a strong bend has been induced at the asparagine residue of the NP motif. The bend is close to $90^\circ$, as compared to $135^\circ$ in the starting structure [72]. The short C-terminal helical segment of TMS7 lies at the acyl chain/headgroup interface, almost parallel to the bilayer surface (Fig. 7). Most of the amino acid residues of the peptide seem to be buried in the acyl chain hydrocarbon region of the bilayer. However, as shown in Fig. 8, the termini of the helix are approximately positioned in the glycerol region. It is also noteworthy (Fig. 8) that on the time scale of 2.5 ns, water molecules rarely penetrate beyond the polar environment of the DMPC bilayer, except perhaps at the C-terminal half of the peptide (see below).

*Lipid bilayer structure.* As seen from the results in Table II, the overall structure of the DMPC bilayer is not very sensitive to the presence of the helical peptide. Thus, the average distance between the phosphatidylcholine groups, the average hydrophobic region thickness, and the average percentage of acyl chain C–C bonds in the *gauche* conformation are all close to the values found for the pure bilayers. Furthermore, the lipid polar group orientation and internal conformation within the membrane-peptide complexes do not differ significantly from pure membrane patches (see Table III). The headgroup dihedral angle conformations of the lipids surrounding the transmembrane peptide also do not differ significantly from those of the NVE-CUT calculation (figure not shown). Particularly, the probability of the *trans* conformation for the $\alpha_1$ dihedral angle is still lower than that for *gauche*+. It is noteworthy, however, that perhaps because of the longer simulation time in the membrane-helix complex, the dihedral angle $\alpha_1$ exhibits about 13% higher percentage of *trans* conformation than within the pure lipids, which brings it closer to the experimentally determined structural parameter.

To determine the effect of TMS7 on the lipid acyl chain orientation, we identified the DMPC acyl chains with an overall minimum distance from the embedded peptide of $<5$ Å and compared their orientational order parameters to those of the other acyl chains with a distance $>5$ Å from the peptide (Fig. 9). From the $2 \times 44$ acyl chains, we have found 31 in contact with the embedded TMS7 peptide. Figure 9 shows that the "contact" lipids have slightly higher orientational order parameters (particularly the Sn-2 chains) and thus appear to be more parallel to the bilayer normal than the "bulk" acyl chains. *This result seems to*

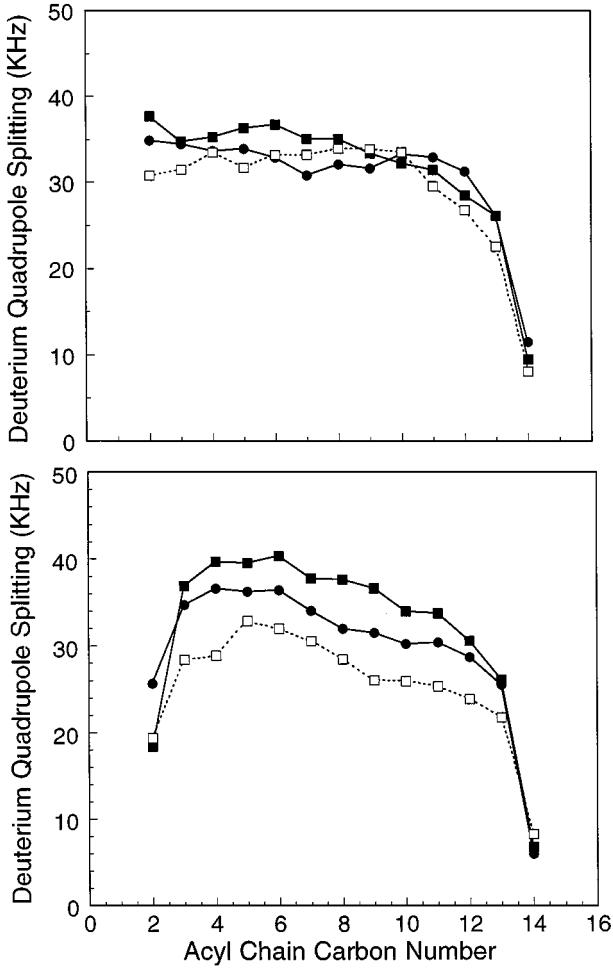


**FIG. 9.** Deuterium quadrupole splitting at different hydrocarbon positions of the DMPC acyl chains Sn-1 (top) and Sn-2 (bottom) for the NVE-CUT (circle) and NVE-CUT-TMS7 (square) simulations. Acyl chains in contact with the TMS7 peptide are displayed with solid lines and closed symbols, whereas those not in contact with TMS7 are represented by dotted lines and open symbols.

*indicate the existence of a "first shell" of lipid acyl chains surrounding the transmembrane helix (but not necessarily a first shell of lipids).* This finding is in good agreement with several experimental studies, which have identified effects of transmembrane peptides on the order of their surrounding lipid acyl chains [28, 30].

*Transmembrane peptide structure.* The time evolution of the RMS deviations from the starting structure is shown in Fig. 10. The RMS deviations converge to a plateau value around 1.3 ns into the simulation, indicating that the system has reached an equilibrium that appears to be stable for the rest of the trajectory. It is also noted that the helix undergoes some structural change starting at about 700 ps that appears to be completed by about 1300 ps. The structural change indicated in Fig. 10 is reflected in the time-evolution of the tilting and bending of the transmembrane helix: Starting at about 1.2 ns of simulation the TMS7 develops an increase in the bend of the NP motif from about 60° to 80° (see Fig. 10) that appears to be completed in around 150–200 ps. Interestingly the bending

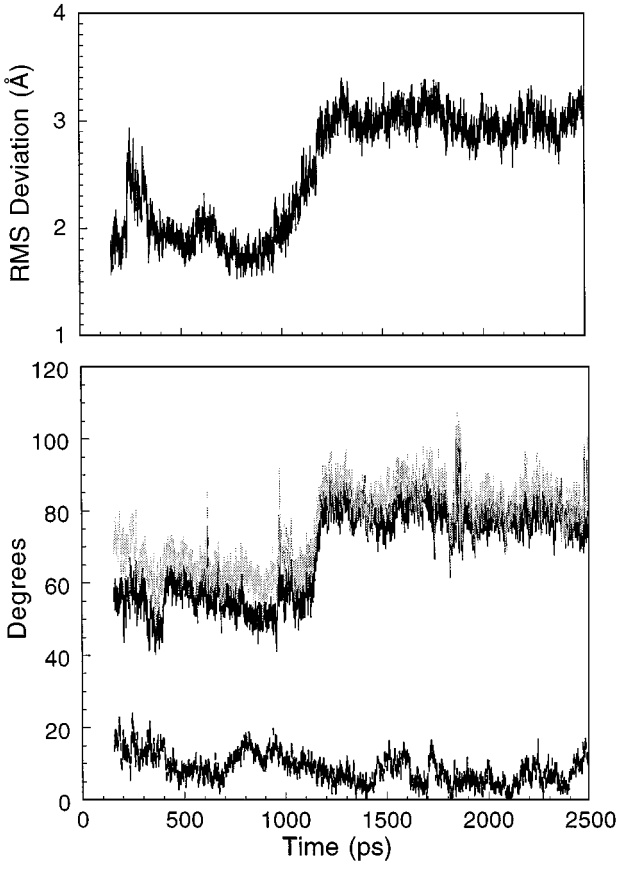


**FIG. 10.** Time evolution of the (all heavy atom) RMS deviation from the starting structure (upper panel) and of the helical axes angles of TMS7 (lower panel): The angle between the helix axis of residues 1–15 and the bilayer normal (dashed, black line), the angle between the helix axis of residues 17–25 and the bilayer normal (solid black line), and the interhelical axes angle (gray line).

process occurs via a reorientation of the short C-terminal helical segment (from residue 17 to 25) almost parallel to the bilayer surface, whereas the long N-terminal helical segment remains approximately parallel to the bilayer normal (Fig. 10).

The helical characters of the peptide can be quantified from the values of the main chain $\Phi$ and $\Psi$ angles; the results are given in Fig. 11. The values of $\Phi$ and $\Psi$ calculated from the last 500 ps of the simulation are all in the range of classical $\alpha$-helices (from $-100^\circ$ to $-40^\circ$ for $\Phi$ and from $-60^\circ$ to $-20^\circ$ for $\Psi$), except for the $\Psi$ angles of $VAL_{15}$ and $ASN_{16}$ which are about $18^\circ$ and $137^\circ$, respectively. These particular values yield an internal conformation of the TMS7 peptide that is in excellent agreement with the main conclusions of an NMR study performed on an isolated 15 residue transmembrane segment of the GPCR tachykinin NK-1 helix 7, which has a very similar sequence to that of TMS7 [17]. In addition, the side chain $X_1$ torsion of residue $ASN_{16}$ remains in a *trans* conformation for the entire MD simulation. Considering also that the fluctuations in structural parameters are very small, as shown in Fig. 11, we can suggest more precisely (Table IV) that the MD calculated TMS7 structure has an internal conformation that is quite close to the structure **2** deduced from NOE constraints measured in a perfluoro-tert-butanol/$CD_3OD$ solvent of the NK-1

**TABLE IV**

**NP Motif Backbone $\phi$ and $\psi$ Dihedral Angles (in Degrees) for the MD-Simulated TMS7 and the Tachykinin NK-1 Helix 7 Structure 2 Deduced from NMR Data [7]**

| TMS7 | | | NK-1 helix | | |
|---|---|---|---|---|---|
| | Φ | Ψ | | Φ | Ψ |
| SER13 | −74 | −39 | THR5 | −62 | −40 |
| ALA14 | −63 | −34 | MET6 | −68 | −18 |
| VAL15 | −86 | 18 | TYR7 | −71 | 64 |
| ASN16 | −93 | 137 | ASN8 | −132 | 112 |
| PRO17 | −69 | −11 | PRO9 | −43 | −36 |
| LEU18 | −78 | −38 | ILE10 | −65 | −45 |
| VAL19 | −75 | −57 | ILE11 | −75 | −45 |
| TYR20 | −68 | −26 | TYR20 | −53 | −42 |

helix 7 [17]. That study also deduced from the NMR data that the bending of the isolated transmembrane helix 7 should be around 90°, which is not far from the value obtained here for TMS7 after the MD simulation.

Notably the final conformation of TMS7 differs from its initial structure mainly in the values of the $VAL_{15}$ Ψ and the $ASN_{16}$ Φ torsion angles (Fig. 11). As shown in Fig. 12, the time evolution of these two dihedral angles reveals a transition at about 1.0 ns of simulation. Because these dihedral angle transitions occur a few picoseconds before the bending of the helix (Fig. 10), they may be precursors that induce the reorientation of the TMS7 short C-terminal helical segment relative to the bilayer surface. Finally, from the Φ and Ψ dihedral angle fluctuations displayed in Fig. 11, it is noted that on the time scale of 500 ps the high flexibility of the TMS7 peptide is rather localized between the $VAL_{15}$ and $ASN_{16}$ residues rather than within the $NP_{17}$ motif since the fluctuations of the (Φ, Ψ)

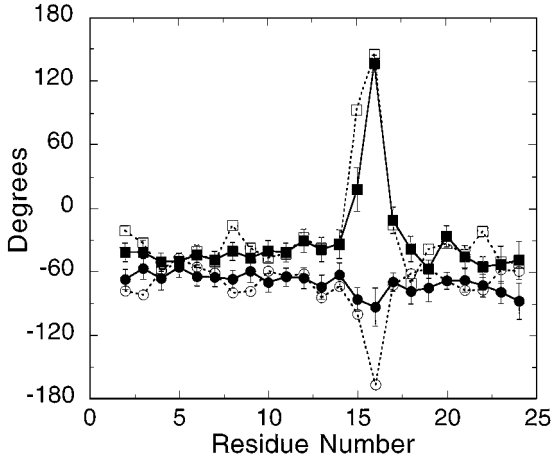


**FIG. 11.** Values and fluctuations of the dihedral angle Φ (closed circle) and Ψ (closed square) for TMS7 residues, averaged over the last 500 ps of simulation. Initial Φ and Ψ values are also displayed with dotted lines and open symbols.

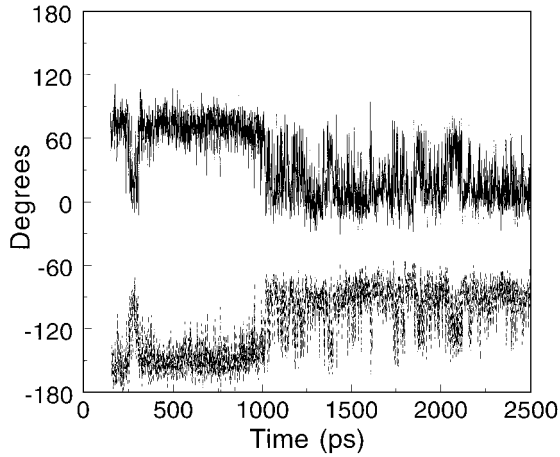


**FIG. 12.** Time evolution of dihedral angles: VAL15 ($\Psi$) (solid line) and ASN16 ($\Phi$) (dashed line).

angles around their mean values are (11°, 20°), (18°, 7°), and (9°, 12°) for $VAL_{15}$, $ASN_{16}$, and $PRO_{17}$, respectively.

*The hydrogen bond network within the membrane-peptide complex.* An overall picture of the hydrogen bond (HB) networks that stabilize the transmembrane helix emerges from Fig. 13, which shows the percentage of time (within the last 500 ps of simulation) for which all peptide HB acceptors and donors are involved in hydrogen bonding. The backbone carbonyl oxygens of the TMS7 C-terminal as well as the backbone NH hydrogens of the N-terminal are partially stabilized by hydrogen bonds with water molecules. The hydroxyl groups of $SER_{12}$ and $SER_{13}$ form HB with the backbone carbonyl oxygens $O_8$ and $O_9$ whereas the $ASN_3$, $TYR_{20}$, and $THR_{21}$ polar side chains are well stabilized by water molecules. Surprisingly, the three polar side chains of $TRP_7$, $TYR_{10}$, and $ASN_{24}$ do not make HB with waters. As shown in Fig. 8 (lower panel), the polar atoms of the side chains of these residues are deeply buried in the hydrophobic region of the membrane. This is expected to result in a lower probability for these residues to be near enough to a water molecule to form a hydrogen bond, explaining the results in Fig. 13. Interestingly, these three side chains are positioned on the face of the peptide that is expected to be oriented toward the interior of the $\alpha$-helix bundle of the receptor protein, and are thus likely to form interhelical HBs [72]. For residues 1 to 11 the $\alpha$-helical $O_i$–$HN_{i+4}$ hydrogen bond stabilities are relatively well preserved. The $O_i$–$HN_{i+4}$ hydrogen bond network is less stable in the C-terminus part of the peptide, but nevertheless, the $\alpha$-helical structure is roughly maintained for the peptide segment from $ASN_{16}$ to the C-terminal end. (Note, however, that the carbonyl oxygen $O_{17}$ prefers to hydrogen bond to the $THR_{21}$ side chain hydroxyl group rather than to the main chain $NH_{21}$ group (Fig. 14).)

Because $PRO_{17}$ does not contribute an NH group, the backbone carbonyl oxygen $O_{13}$ tends to form an $[i-(i+3)]$ hydrogen bond with the NH of $ASN_{16}$. The presence of a proline in the TMS7 sequence also disrupts the $\alpha$-helical hydrogen bonds $O_{14}$–$HN_{18}$ and $O_{15}$–$HN_{19}$. To compensate for these HB breaks, the backbone NH hydrogen of $ASN_{16}$ partially hydrogen bonds to the alanine carbonyl $O_{14}$ (in addition to SER $O_{13}$), while the $ASN_{16}$ side chain carbonyl group forms an HB with the $LEU_{18}$ backbone NH hydrogen (Fig. 14). Instead of the $\alpha$-helical $O_{15}$–$HN_{19}$ hydrogen bond, a $3_{10}$ helix-like hydrogen bond $[i-(i+3)]$ is formed between the $O_{16}$ carbonyl and the backbone NH of the $VAL_{19}$

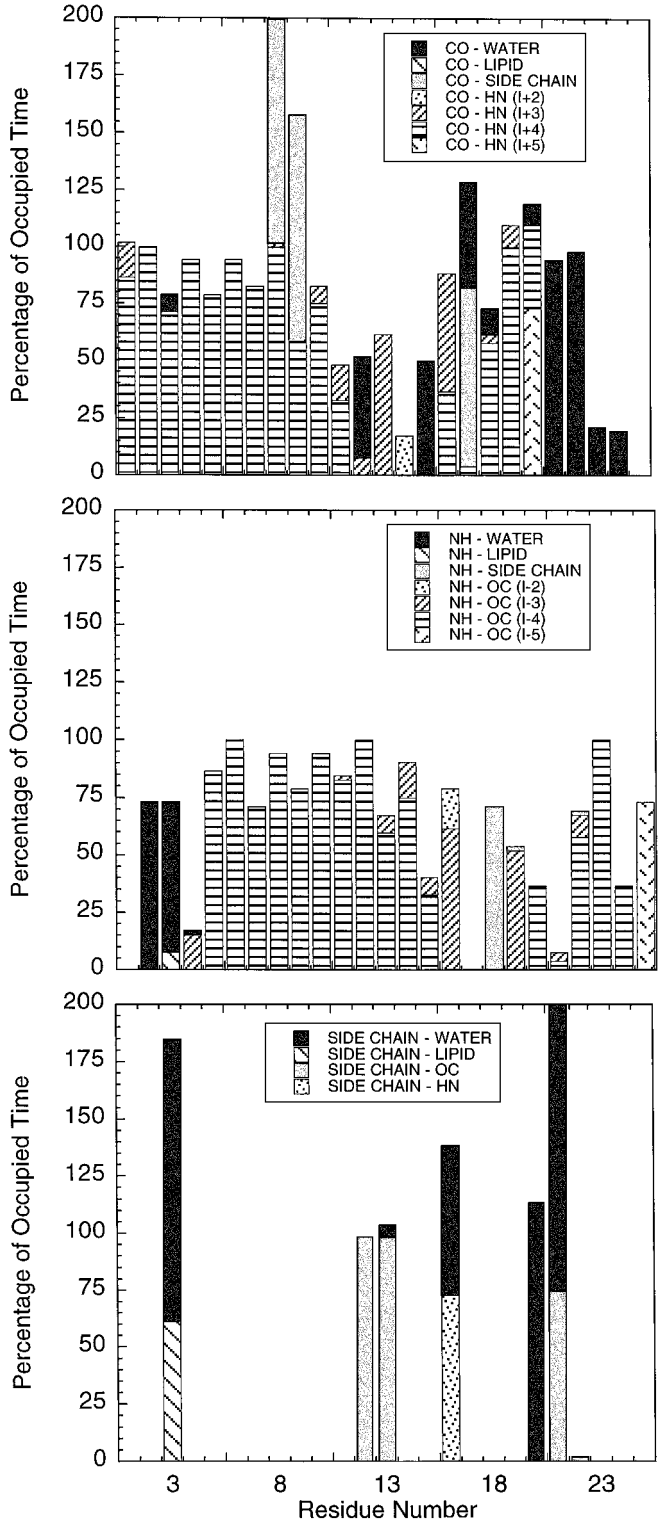


**FIG. 13.** Percentage of time from the last 500 ps of the NVE-CUT-TMS7 simulation in which peptide backbone groups are hydrogen bonded: carbonyl oxygens (top panel, NH hydrogens (middle panel), and polar side chains (bottom panel). A hydrogen bond is considered to be present when the distance between the proton and the acceptor is $<2.5$ Å, and the X-H-Y angle is $>1350$.

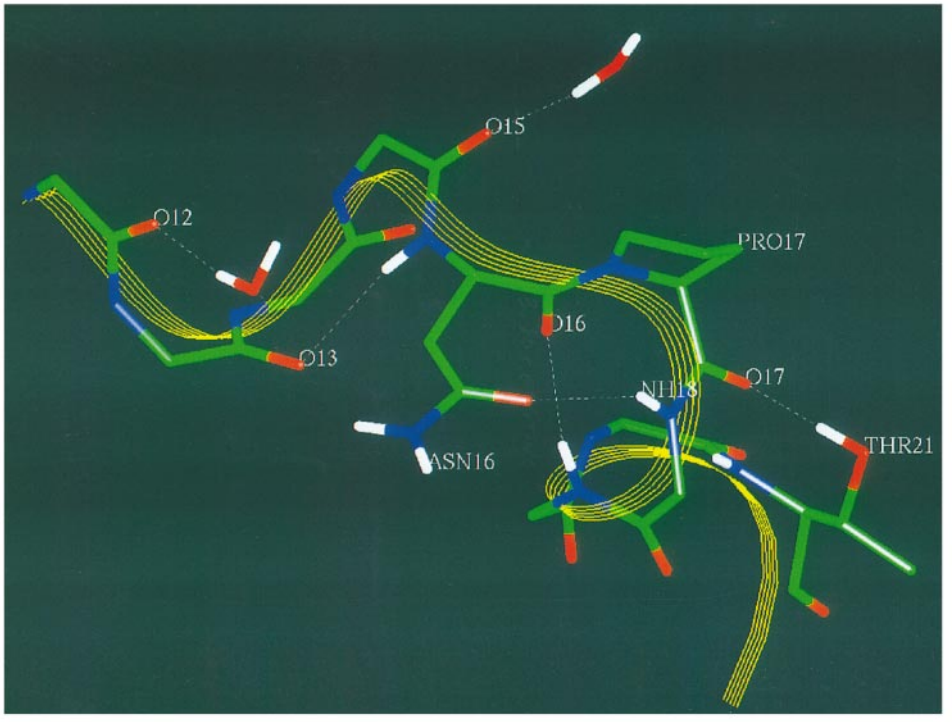


**FIG. 14.** Configuration of the TMS7 hydrogen bond network around the NP motif from a single entry in the trajectory (snapshot) at the end of the NVE-CUT-TMS7 simulation.

backbone NH group. At the same time the lone carbonyl oxygen $O_{15}$ is partially stabilized by a water molecule that has penetrated into the hydrophobic region of the membrane. In addition, it should be noted that the $ASN_{16}$ residue backbone NH hydrogen is involved in hydrogen bonds with the two carbonyl $O_{13}$ and $O_{14}$ oxygens, and therefore can hardly form an $[i-(i+4)]$ hydrogen bond with the $SER_{12}$ backbone carbonyl oxygen. *However, this latter HB is satisfied by a water molecule that has penetrated the membrane deeply enough to provide an hydrogen bond donor to this backbone carbonyl oxygen about 50% of the time* (Figs. 13 and 14).

It is significant that the main features of the TMS7 intramolecular hydrogen bonding pattern predicted by the MD simulations are in good agreement with the HBs deduced from the NMR data obtained on the tachykinin NK-1 helix 7 in a perfluoro-tert-butanol/$CD_3OD$ solvent [17]. In particular, the NH backbone group of residue $ASN_8$ in tachykinin NK-1, which corresponds to $ASN_{16}$ in TMS7, is predicted to form hydrogen bonds of type $[i-(i+2)]$ and $[i-(i+3)]$ with $MET_6$ and $THR_5$ backbone carbonyl oxygens. Similarly to TMS7, the NK-1 helix backbone carbonyl oxygen $O_8$ forms both $[i-(i+3)]$ and $[i-(i+4)]$ HB with NH amide groups of residues $ILE_{11}$ and $TYR_{12}$ (which correspond to the residues $VAL_{19}$ and $TYR_{20}$, respectively, in TMS7). In addition, it is found experimentally that the side chain of residue $ASN_8$ forms an HB with the proton of the NH group in $ILE_{10}$ as was found here between the residues $ASN_{16}$ and $LEU_{18}$ of the TMS7 peptide. Finally, it is noted that for both of these similar transmembrane segments, the backbone carbonyl oxygen of the proline tends to form an HB with the side chain of the fourth succeeding residue, which is respectively the $SER_{13}$ and $THR_{21}$ in the NK-1 and TMS7 peptides [17].

**TABLE V**
**Hydrogen Bond Distances (Å) around the TMS7 Peptide NP Motif**

| Expected [i−(i + 4)] HB | Initial structure | Last 500 Ps average | Instead observed HB | Initial structure | Last 500 Ps average |
|---|---|---|---|---|---|
| O12–HN16 | 5.8 | 4.3 | O12–OH2 | — | 4.7 |
| O13–HN17 | — | — | O13–HN16 | 4.7 | 2.5 |
| O14–HN18 | 6.3 | 6.8 | O14–HN16 | 2.6 | 2.8 |
| | | | OD16–HN18 | 2.8 | 2.4 |
| O15–HN19 | 6.8 | 6.3 | O15–OH2 | — | 3.9 |
| | | | O16–HN19 | 3.4 | 2.4 |

The average lengths of some of the crucial hydrogen bonds that stabilize the NP motif of TMS7 are reported in Table V. The distances of $O_{12}$–$HN_{16}$ and $O_{13}$–$HN_{16}$ are shown to have decreased most from the initial TMS7 structure, suggesting that the backbone NH group of $ASN_{16}$, which originally forms an $[i-(i+2)]$ hydrogen bond with the carbonyl oxygen $O_{14}$ [72], has a strong tendency to interact with the two preceding carbonyl oxygens of residues 12 and 13 to form more common $[i-(i+3)]$ and $[i-(i+4)]$ hydrogen bonds. Furthermore, the time evolution of these two distances (Fig. 15) shows a transition around 1 ns for both of them that indicates the formation of a weak HB with $O_{12}$ and a normal one with the $O_{13}$ atom. Thus, it seems that the local hydrogen bonding interactions between the carbonyl oxygens $O_{12}$, $O_{13}$, and $O_{14}$ and the backbone NH group of $ASN_{16}$ are precursors for the local transitions of the $VAL_{15}$ $\Psi$ and the $ASN_{16}$ $\Phi$ torsion angles identified in Fig. 12. These transitions are likely responsible for inducing the subsequent global reorientation of the C-terminal helical segment of TMS7 (Fig. 10).

*Water penetration into the membrane.* As seen in the previous section, some water molecules penetrate into the hydrophobic region of the DMPC bilayer where they can form hydrogen bonds with acceptor and donor residues in TMS7 that have no other partner. The average number of water molecules in the bilayer hydrophobic region calculated from the last 500 ps of the simulation is presented in Fig. 16. *The presence of the peptide clearly allows significantly more water molecules to penetrate the bilayer than in the case of the pure membrane*. However, this observation seems to be true only for the C-terminal segment, perhaps because it penetrates more deeply into the lipid polar headgroup region than the N-terminal ends (Fig. 7). Considering that the hydrophobic regions of the membrane extend from −7 to 7 Å, as shown in Fig. 8, the last 500 ps of the simulations reveals that roughly one water molecule can consistently penetrate the hydrocarbon regions of the membrane in the presence of the peptide (Fig. 16). This finding of water molecules in the membrane hydrophobic region close to the peptides is consistent with results from several experimental studies that reveal the presence of water at the peptide-lipid hydrophobic interface of various membrane-protein complexes [99–101].

Figure 17 illustrates the difference in water penetration behavior between the peptide-containing bilayer (NVE-CUT-TMS7) and pure membrane (NVE-CUT). The positions of the water molecules that penetrate the deepest into the lipid hydrocarbon region are displayed along the bilayer normal as a function of time. Notably, in the pure membrane a water molecule entering the hydrophobic region does not remain there longer than a few picoseconds and then returns very rapidly to the lipid glycerol region (around ±10 Å). In

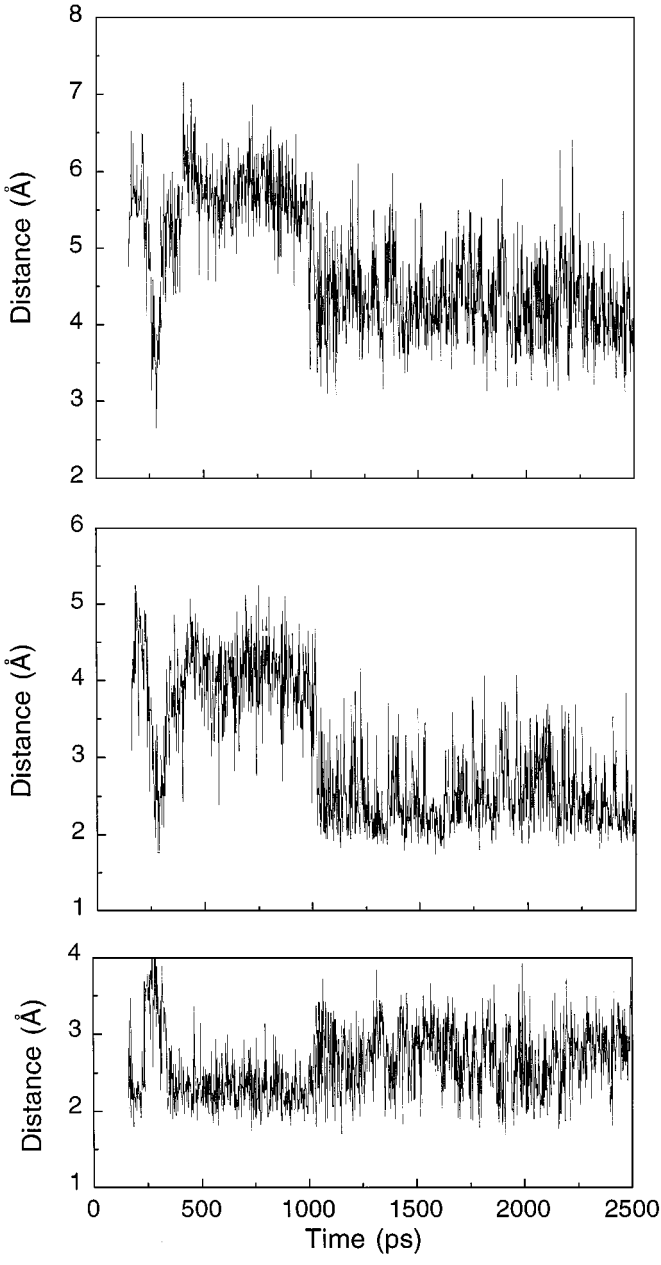


**FIG. 15.** Time dependence of the distances between the ASN16 backbone NH group and the carbonyl oxygen of the SER12 (top panel), SER13 (middle panel), and ALA14 (bottom panel) in the TMS7 peptide.

contrast, the NVE-CUT-TMS7 simulation reveals one water molecule ($W_{1682}$) that remains in the lipid hydrocarbon region for several hundred picoseconds. This water molecule is strongly hydrogen bonded to the $SER_{12}$ backbone carbonyl oxygen (Fig. 14) and to a lesser extent to the backbone oxygen of $VAL_{15}$. (Note that three different water molecules that penetrate into the membrane were found to stabilize successively the backbone carbonyl oxygen $O_{15}$.)

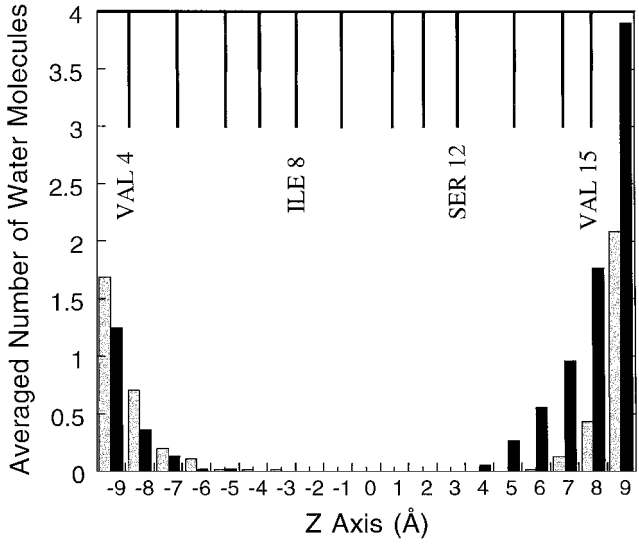


**FIG. 16.** Averaged number of water molecules present at different depths of the membrane hydrophobic region for the NVE-CUT (gray) and NVE-CUT-TMS7 (black) simulations. Upper solid lines show average positions of backbone carbonyl oxygens for residues 4–15 of TMS7.

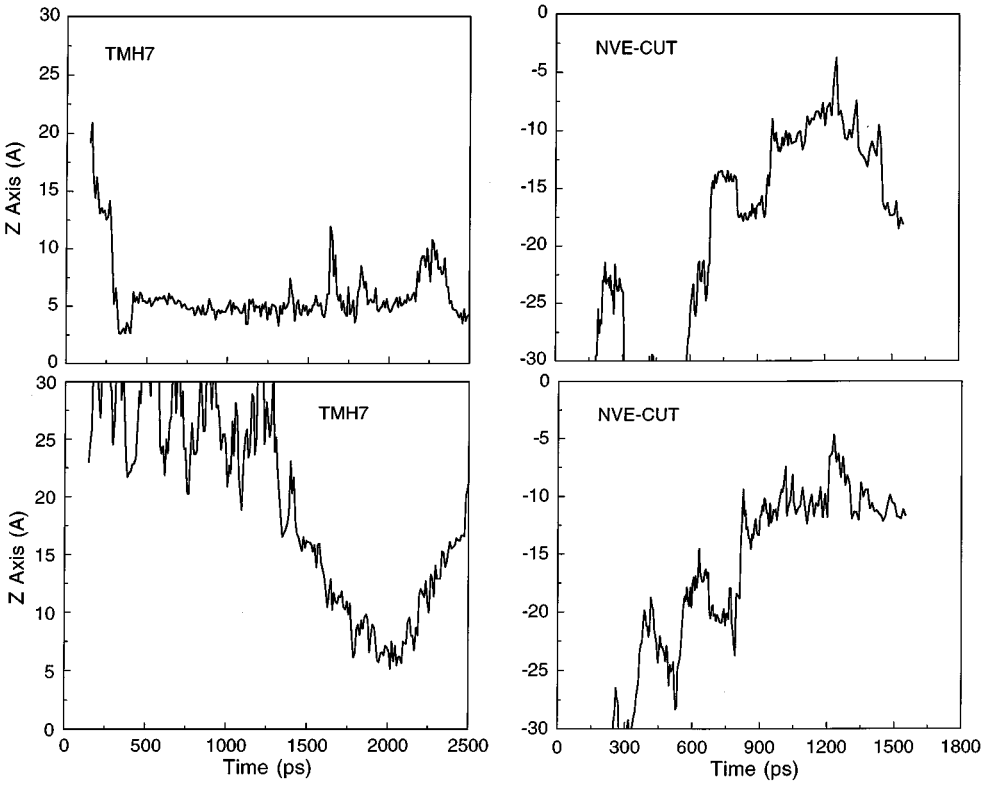


**FIG. 17.** Time evolution of the positions of two water molecules in the membrane bilayer represented along the membrane bilayer normal for the NVE-CUT and TMS7 systems.

## CONCLUSIONS

Three separate 1.5-ns molecular dynamics simulations under different computational conditions (NVE-CUT, NPT-CUT, and NPT-EXT) were performed on pure DMPC bilayers in the liquid-crystalline phase. Averages from the last 500 ps of the simulations were used to estimate various properties of the bilayer and compared to available experimental values for the overall geometrical dimensions, lipid hydrocarbon chain ordered states, and polar head group conformations. The agreement with experiment is good in spite of some discrepancies that probably result from shortcomings in the force field and, in some cases, to the short MD production runs. It is interesting to note that this agreement with experimental data is quite robust. This is indicated by comparisons in Table II showing that the differences among results obtained with the three computational models employed here are smaller than the corresponding differences among experimental measurements. Notably, the fluctuations of such values for structural parameters calculated from the simulations were found to be very small (e.g., see Fig. 11 for results with the NVE-CUT model). The results of this comparative study suggest that the simulation carried out in the microcanonical ensemble using truncated electrostatic interactions yielded more reasonable descriptions of the membrane structure than the two constant pressure calculations. However, in order to obtain reasonable, stable results in the microcanonical ensemble, it has proven essential for the systems to be allowed to equilibrate fully. This may often require considerable trajectory time, the length of which cannot be predicted a priori.

The good agreement with available experimental data pertains also to the study of the peptide-membrane complex. The resulting equilibrated and averaged structure of the membrane spanning peptide TMS7 of the 5-$HT_{2A}$ receptor comprises two $\alpha$-helical segments linked by a hinge domain around $ASN_{16}$-$PRO_{17}$ residues. The details of this conformation, including the hydrogen bond network and the bend angle, were found to be in good agreement with the structure of the tachykinin NK-1 receptor helix 7 deduced from NMR data [17], as well as with the known structural considerations about this transmembrane domain (for details see [72]). Both the properties of the membrane lipids surrounding the peptide and the stabilizing role of individual water molecules that are found to penetrate the membrane bilayer agree with experimental observations from similar systems. These findings further support evidence from other studies that MD simulations can predict reasonable structures of membrane-peptide complexes.

The details of the observed hydrogen bond organization strongly suggest that lipid bilayers stabilize even single transmembrane helical segments that contain a structure-disrupting proline. In part, this stabilization is realized with the help of a few water molecules that penetrate into the membrane hydrophobic region. This penetration is more pronounced in the peptide-membrane complex than in the pure membrane patches. An additional factor that may influence stability is the significant difference found here between the orientational order parameters of lipid acyl chain neighboring transmembrane helices and those of "bulk" lipid acyl chains. This effect results from van der Waals interactions between parts of the transmembrane peptide and surrounding lipid hydrocarbon chains and seems to depend on the orientation of the helices. It will be important to explore these local arrangements and the resulting interactions with the membrane and water, for a complete GPCR structure imbedded in a membrane patch. These key elements of protein-membrane interactions are likely to affect the structural organization of the proteins containing seven transmembrane segments, as well as their function.

## ACKNOWLEDGMENTS

The authors thank Dr. Benoit Roux for providing the protocols developed in his laboratory for the construction of membrane patches, and for his generous assistance in the early stages of our studies. Computational support was provided by the Cornell Supercomputer Facility and the Advanced Scientific Computing Laboratory at the Frederick Cancer Research Facility of the National Cancer Institute (Laboratory for Mathematical Biology). This work was supported by the National Institutes of Health Grants R01 DA09083, DK46943, and K05 DA00060.

## REFERENCES

1. T. W. Kahn and D. M. Engelman, Bacteriorhodopsin can be refolded from two independently stable transmembrane helices and the complementary five-helix fragment, *Biochemistry* **31**, 6144 (1992).
2. J. L. Popot and D. M. Engelman, Membrane protein folding and oligomerization: The two-stage model, *Biochemistry* **29**, 4031 (1990).
3. T. B. Woolf, Molecular dynamics simulations of individual alpha-helices of bacteriorhodopsin in dimyristoylphosphatidylcholine. II. Interaction energy analysis, *Biophys. J.* **74**, 115 (1998).
4. S. Berneche, M. Nina, and B. Roux, Molecular Dynamics simulation of melittin in a dimyristoylphosphatidylcholine bilayer membrane, *Biophys. J.* **75**, 1603 (1998).
5. M. F. Brown, Modulation of rhodopsin function by properties of the membrane bilayer, *Chem. Phys. Lipids* **73**, 159 (1994).
6. R. L. Cornea and D. D. Thomas, Effects of membrane thickness on the molecular dynamics and enzymatic activity of reconstituted Ca-ATPase, *Biochemistry* **33**, 2912 (1994).
7. H. L. Casal and R. N. McElhaney, Quantitative determination of hydrocarbon chain conformational order in bilayers of saturated phosphatidylcholines of various chain lengths by Fourier transform infrared spectroscopy, *Biochemistry* **29**, 5423 (1990).
8. R. Mendelsohn, M. A. Davies, J. W. Brauner, H. F. Schuster, and R. A. Dluhy, Quantitative determination of conformational disorder in the acyl chains of phospholipid bilayers by infrared spectroscopy, *Biochemistry* **28**, 8934 (1989).
9. T. Mavromoustakos, D. P. Yang, A. Charalambous, L. G. Herbette, and A. Makriyannis, Study of the topography of cannabinoids in model membranes using x-ray diffraction, *Biochim. Biophys. Acta* **1024**, 336 (1990).
10. J. F. Nagle, R. Zhang, S. Tristram-Nagle, W. Sun, H. I. Petrache, and R. M. Suter, X-ray structure determination of fully hydrated L alpha phase dipalmitoylphosphatidylcholine bilayers, *Biophys. J.* **70**, 1419 (1996).
11. M. C. Wiener and S. H. White, Structure of a fluid dioleoylphosphatidylcholine bilayer determined by joint refinement of x-ray and neutron diffraction data. III. Complete structure, *Biophys. J.* **61**, 437 (1992).
12. C. Morrison and M. Bloom, Orientation dependence of $^2$H nuclear magnetic resonance spin-lattice relaxation in phospholipid and phospholipid: Cholesterol systems, *J. Chem. Phys.* **101**, 749 (1994).
13. D. Rice and E. Oldfield, Deuterium nuclear magnetic resonance studies of the interaction between dimyristoylphosphatidylcholine and gramicidin A′, *Biochemistry* **18**, 3272 (1979).
14. C. R. Sanders, Solid state 13C NMR of unlabeled phosphatidylcholine bilayers: Spectral assignments and measurement of carbon-phosphorus dipolar couplings and 13C chemical shift anisotropies, *Biophys. J.* **64**, 171 (1993).
15. J. Seelig and A. Seelig, Lipid conformation in model membranes and biological membranes, *Q. Rev. Biophys.* **13**, 19 (1980).
16. B. Bechinger, Structure and dynamics of the M13 coat signal sequence in membranes by multidimensional high-resolution and solid-state NMR spectroscopy, *Proteins* **27**, 481 (1997).
17. J. P. Berlose, O. Convert, A. Brunissen, G. Chassaing, and S. Lavielle, Three-dimensional structure of the highly conserved seventh transmembrane domain of G-protein-coupled receptors, *Eur. J. Biochem.* **225**, 827 (1994).

18. T. A. Cross and S. J. Opella, Solid-state NMR structural studies of peptides and proteins in membranes, *Curr. Opin. Struct. Biol.* **4**, 574 (1994).
19. E. Gazit, I. R. Miller, P. C. Biggin, M. S. Sansom, and Y. Shai, Structure and orientation of the mammalian antibacterial peptide cecropin P1 within phospholipid membranes, *J. Mol. Biol.* **258**, 860 (1996).
20. H. H. De Jongh, R. Brasseur, and J. A. Killian, Orientation of the alpha-helices of apocytochrome c and derived fragments at membrane interfaces, as studied by circular dichroism, *Biochemistry* **33**, 14,529 (1994).
21. H. W. Huang, Structural basis and energetics of peptide membrane interactions, in *Biological Membranes*, edited by K. M. Merz, Jr., and B. Roux (Birkhäuser, Boston, 1996), p. 281.
22. C. Gray and L. K. Tamm, Structural studies on membrane-embedded influenza hemagglutinin and its fragments, *Protein Sci.* **6**, 1993 (1997).
23. Y. P. Zhang, R. N. Lewis, G. D. Henry, B. D. Sykes, R. S. Hodges, and R. N. McElhaney, Peptide models of helical hydrophobic transmembrane segments of membrane proteins. 1. Studies of the conformation, intrabilayer orientation, and amide hydrogen exchangeability of Ac-K2-(LA)12-K2- amide, *Biochemistry* **34**, 2348 (1995).
24. H. Vogel, L. Nilsson, R. Rigler, K. P. Voges, and G. Jung, Structural fluctuations of a helical polypeptide traversing a lipid bilayer, *Proc. Natl. Acad. Sci. U.S.A.* **85**, 5067 (1988).
25. W. Hu, N. D. Lazo, and T. A. Cross, Tryptophan dynamics and structural refinement in a lipid bilayer environment: Solid state NMR of the gramicidin channel, *Biochemistry* **34**, 14,138 (1995).
26. J. A. Killian, I. Salemink, M. R. de Planque, G. Lindblom, R. E. Koeppe, 2nd, and D. V. Greathouse, Induction of nonbilayer structures in diacylphosphatidylcholine model membranes by transmembrane alpha-helical peptides: Importance of hydrophobic mismatch and proposed role of tryptophans, *Biochemistry* **35**, 1037 (1996).
27. S. Morein, E. Strandberg, J. A. Killian, S. Persson, G. Arvidson, R. E. Koeppe, 2nd, and G. Lindblom, Influence of membrane-spanning alpha-helical peptides on the phase behavior of the dioleoylphosphatidylcholine/water system, *Biophys. J.* **73**, 3078 (1997).
28. W. K. Subczynski, R. N. Lewis, R. N. McElhaney, R. S. Hodges, J. S. Hyde, and A. Kusumi, Molecular organization and dynamics of 1-palmitoyl-2-oleoylphosphatidylcholine bilayers containing a transmembrane alpha- helical peptide, *Biochemistry* **37**, 3156 (1998).
29. T. C. Vogt, J. A. Killian, and B. De Kruijff, Structure and dynamics of the acyl chain of a transmembrane polypeptide, *Biochemistry* **33**, 2063 (1994).
30. Y. P. Zhang, R. N. Lewis, R. S. Hodges, and R. N. McElhaney, Peptide models of helical hydrophobic transmembrane segments of membrane proteins. 2. Differential scanning calorimetric and FTIR spectroscopic studies of the interaction of Ac-K2-(LA)12-K2-amide with phosphatidylcholine bilayers, *Biochemistry* **34**, 2362 (1995).
31. M. M. Sperotto and O. G. Mouritsen, Monte Carlo simulation studies of lipid order parameter profiles near integral membrane proteins, *Biophys. J.* **59**, 261 (1991).
32. T. Heimburg and R. L. Biltonen, A Monte Carlo simulation study of protein-induced heat capacity changes and lipid-induced protein clustering, *Biophys. J.* **70**, 84 (1996).
33. J. Skolnick and M. Milik, Monte carlo models of spontaneous insertion of peptides into lipid membranes, in *Biological Membranes*, edited by K. M. Merz, Jr., and B. Roux (Birkhäuser, Boston, 1996), p. 535.
34. O. Berger, O. Edholm, and F. Jahnig, Molecular dynamics simulations of a fluid bilayer of dipalmitoylphosphatidylcholine at full hydration, constant pressure, and constant temperature, *Biophys. J.* **72**, 2002 (1997).
35. S. W. Chiu, M. Clark, V. Balaji, S. Subramaniam, H. L. Scott, and E. Jakobsson, Incorporation of surface tension into molecular dynamics simulation of an interface: A fluid phase lipid bilayer membrane, *Biophys. J.* **69**, 1230 (1995).
36. J. W. Essex, M. M. Hann, and W. G. Richards, Molecular dynamics simulation of a hydrated phospholipid bilayer, *Philos. Trans. R. Soc. London B Biol. Sci.* **344**, 239 (1994).
37. S. E. Feller, D. Yin, R. W. Pastor, and A. D. MacKerell, Jr., Molecular dynamics simulation of unsaturated lipid bilayers at low hydration: Parameterization and comparison with diffraction studies, *Biophys. J.* **73**, 2269 (1997).

38. M. T. Hyvonen, T. T. Rantala, and M. Ala-Korpela, Structure and dynamic properties of diunsaturated 1-palmitoyl-2-linoleoyl-sn-glycero-3-phosphatidylcholine lipid bilayer from molecular dynamics simulation, *Biophys. J.* **73**, 2907 (1997).
39. E. Jakobsson, Computer simulation studies of biological membranes: Progress, promise and pitfalls, *Trends Biochem. Sci.* **22**, 339 (1997).
40. K. M. Merz, Jr., Molecular dynamics simulations of lipid bilayers, *Curr. Opin. Struct. Biol.* **7**, 511 (1997).
41. R. W. Pastor, Molecular dynamics and monte carlo simulations of lipid bilayers, *Curr. Opin. Struct. Biol.* **4**, 486 (1994).
42. A. J. Robinson, W. G. Richards, P. J. Thomas, and M. M. Hann, Head group and chain behavior in biological membranes: A molecular dynamics computer simulation. *Biophys. J.* **67**, 2345 (1994).
43. W. Shinoda, N. Namiki, and S. Okazaki, Molecular dynamics study of a lipid bilayer: Convergence, structure and long-time dynamics, *J. Chem. Phys.* **106**, 5731 (1997).
44. D. P. Tieleman and H. J. C. Berendsen, Molecular dynamics simulations of a fully hydrated dipalmitoylphosphatidylcholine bilayer with different macroscopic boundary conditions and parameters, *J. Chem. Phys.* **105**, 4871 (1996).
45. D. P. Tieleman, S. J. Marrink, and H. J. Berendsen, A computer perspective of membranes: Molecular dynamics studies of lipid bilayer systems, *Biochim. Biophys. Acta* **1331**, 235 (1997).
46. K. Tu, D. J. Tobias, and M. L. Klein, Constant pressure and temperature molecular dynamics simulation of a fully hydrated liquid crystal phase dipalmitoylphosphatidylcholine bilayer, *Biophys. J.* **69**, 2558 (1995).
47. R. M. Venable, Y. Zhang, B. J. Hardy, and R. W. Pastor, Molecular dynamics simulations of a lipid bilayer and of hexadecane: An investigation of membrane fluidity, *Science* **262**, 223 (1993).
48. F. Zhou and K. Schulten, Molecular dynamics study of a membrane-water interface, *J. Phys. Chem.* **99**, 2194 (1995).
49. O. Edholm, O. Berger, and F. Jahnig, Structure and fluctuations of bacteriorhodopsin in the purple membrane: A molecular dynamics study, *J. Mol. Biol.* **250**, 94 (1995).
50. T. B. Woolf and B. Roux, Structure, energetics, and dynamics of lipid-protein interactions: A molecular dynamics study of the gramicidin A channel in a DMPC bilayer, *Proteins* **24**, 92 (1996).
51. B. Roux and T. B. Woolf, Molecular dynamics of Pf1 coat protein in a phospholipid bilayer, in *Biological Membranes*, edited by K. M. Merz, Jr., and B. Roux (Birkhäuser, Boston, 1996), p. 555.
52. D. R. Garmer, MD simulations of a 5-HT2A receptor model in DOPC membranes, *J. Biomol. Struct. Dyn.* **14**, 525 (1997).
53. D. P. Tieleman and H. J. Berendsen, A molecular dynamics study of the pores formed by Escherichia coli OmpF porin in a fully hydrated palmitoyloleoylphosphatidylcholine bilayer, *Biophys. J.* **74**, 2786 (1998).
54. K. Belohorcova, J. H. Davis, T. B. Woolf, and B. Roux, Structure and dynamics of an amphiphilic peptide in a lipid bilayer: A molecular dynamics study, *Biophys. J.* **73**, 3039 (1997).
55. O. Edholm and J. Johansson, Lipid bilayer polypeptide interactions studied by molecular dynamics simulation, *Eur. Biophys. J.* **14**, 203 (1987).
56. P. Huang and G. H. Loew, Interaction of an amphiphilic peptide with a phospholipid bilayer surface by molecular dynamics simulation study, *J. Biomol. Struct. Dyn.* **12**, 937 (1995).
57. V. Kothekar, K. Mahajan, K. Raha, and D. Gupta, Molecular dynamics simulation of conformational flexibility of alamethicin fragments in aqueous and membranous environment, *J. Biomol. Struct. Dyn.* **14**, 303 (1996).
58. L. Shen, D. Bassolino, and T. Stouch, Transmembrane helix structure, dynamics, and interactions: Multinanosecond molecular dynamics simulations, *Biophys. J.* **73**, 3 (1997).
59. T. B. Woolf, Molecular dynamics of individual alpha-helices of bacteriorhodopsin in dimyristol phosphatidylocholine. I. Structure and dynamics, *Biophys. J.* **73**, 2376 (1997).
60. X. Luo, D. Zhang, and H. Weinstein, Ligand-induced domain motion in the activation mechanism of a G-protein-coupled receptor, *Protein Eng.* **7**, 1441 (1994).
61. D. Zhang and H. Weinstein, Signal transduction by a 5-HT2 receptor: A mechanistic hypothesis from molecular dynamics simulations of the three-dimensional model of the receptor complexed to ligands, *J. Med. Chem.* **36**, 934 (1993).

62. D. Fu, J. A. Ballesteros, H. Weinstein, J. Chen, and J. Javitch, Residues in the seventh membrane-spanning segment of the dopamine D2 receptor accessible in the binding-site crevice, *Biochemistry* **35**(35), 11,278 (1996).
63. C. M. Deber, M. Glibowicka, and G. A. Woolley, Conformations of proline residues in membrane environments, *Biopolymers* **29**, 149 (1990).
64. R. Sankararamakrishnan and S. Vishveshwara, Characterization of proline-containing alpha-helix (helix F model of bacteriorhodopsin) by molecular dynamics studies, *Proteins* **15**, 26 (1993).
65. R. Sankararamakrishnan and M. S. Samsom, Kinked structures of isolated nicotinic receptor M2 helices: A molecular dynamics study, *Biopolymers* **34**, 1647 (1994).
66. J. Wess, S. Nanavati, Z. Vogel, and R. Maggio, Functional role of proline and tryptophan residues highly conserved among G protein-coupled receptors studied by mutational analysis of the m3 muscarinic receptor, *Embo. J.* **12**, 331 (1993).
67. K. A. Williams and C. M. Deber, Proline residues in transmembrane helices: Structural or dynamic role? *Biochemistry* **30**, 8919 (1991).
68. R. H. Yun, A. Anderson, and J. Hermans, Proline in alpha-helix: Stability and conformation studied by dynamics simulation, *Proteins* **10**, 219 (1991).
69. J. A. Ballesteros and H. Weinstein, Integrated methods for the construction of three-dimensional models and computational probing of structure-function relations in G protein-coupled receptors, *Meth. Neurosci.* **25**, 366 (1995).
70. R. H. Stote, D. J. States, and M. Karplus, *J. Chim. Phys.* **11**, (1991).
71. M. Sundaralingam, Discussion paper: Molecular structures and conformations of the phospholipids and sphingomyelins, *Ann. N. Y. Acad. Sci.* **195**, 324 (1972).
72. K. Konvicka, F. Guarnieri, J. A. Ballesteros, and H. Weinstein, A proposed structure for transmembrane segment 7 of G protein-coupled receptors incorporating an asn-Pro/Asp-Pro motif, *Biophys. J.* **75**, 601 (1998).
73. L. R. De Young, and K. A. Dill, Solute partitioning into lipid bilayer membranes, *Biochemistry* **27**, 5281 (1988).
74. M. J. Janiak, D. M. Small, and G. G. Shipley, Temperature and compositional dependence of the structure of hydrated dimyristoyl lecithin, *J. Biol. Chem.* **254**, 6068 (1979).
75. B. W. Koenig, H. H. Strey, and K. Gawrisch, Membrane lateral compressibility determined by NMR and x-ray diffraction: Effect of acyl chain polyunsaturation, *Biophys. J.* **73**, 1954 (1997).
76. B. A. Lewis and D. M. Engelman, Lipid bilayer thickness varies linearly with acyl chain length in fluid phosphatidylcholine vesicles, *J. Mol. Biol.* **166**, 211 (1983).
77. R. P. Rand and V. A. Parsegian, Hydration forces between phospholipid bilayers, *Biochim. Biophys. Acta.* **988**, 351 (1989).
78. T. B. Woolf and B. Roux, Molecular dynamics simulation of the gramicidin channel in a phospholipid bilayer, *Proc. Natl. Acad. Sci. U.S.A.* **91**, 11,631 (1994).
79. K. M. Merz, Jr., and B. Roux, *Biological Membranes* (Birkhäuser, Boston 1996).
80. B. R. Brooks, R. E. Bruccoleri, B. D. Olafson, D. J. States, S. Swaminathan, and M. Karplus, Charmm: A program for macromolecular energy, minimization and dynamics calculations, *J. Comp. Chem.* **4**, 187 (1983).
81. M. Schlenkrich, J. Brickmann, A. D. MacKerell, Jr., and M. Karplus, An empirical potential energy function for phospholipids: Criteria for parameter optimization and applications, in *Biological Membranes*, edited by K. M. Merz, Jr., and B. Roux (Birkhäuser, Boston, 1996), p. 31.
82. W. L. Jorgensen, J. Chandrasekhar, J. D. Madura, R. W. Impey, and M. L. Klein, Comparison of simple potential functions for simulating liquid water, *J. Chem. Phys.* **79**, 926 (1983).
83. J. P. Ryckaert, C. Cicotti, and H. J. C. Berendsen, *J. Comp. Chem.* **23**, 327 (1977).
84. S. E. Feller, Y. Zhang, R. W. Pastor, and B. R. Brooks, Constant pressure molecular dynamics simulation: The langevin piston method, *J. Chem. Phys.* **103**, 4613 (1995).
85. H. C. Andersen, Molecular dynamics simulations at constant pressure and/or temperature, *J. Chem. Phys.* **72**, 2384 (1980).

86. W. G. Hoover, *Phys. Rev. A* **31**, 1695 (1985).
87. S. Nose, A unified formulation of the constant temperature molecualr dynamics methods, *J. Chem. Phys.* **81**, 511 (1984).
88. M. Caffrey and J. Hogan, LIPIDAT: A database of lipid phase transition temperatures and enthalpy changes, DMPC data subset analysis, *Chem. Phys. Lipids* **61**, 1 (1992).
89. J. F. Nagle and D. A. Wilkinson, Lecithin bilayers: Density measurement and molecular interactions, *Biophys. J.* **23**, 159 (1978).
90. R. H. Pearson and I. Pascher, The molecular structure of lecithin dihydrate, *Nature* **281**, 499 (1979).
91. D. A. Pink, T. J. Green, and D. Chapman, Raman scattering in bilayers of saturated phosphatidylcholines: Experiment and theory, *Biochemistry* **19**, 349 (1980).
92. H. Akutsu and T. Nagamori, Conformational analysis of the polar head group in phosphatidylcholine bilayers: A structural change induced by cations, *Biochemistry* **30**, 4510 (1991).
93. G. Buldt, H. U. Gally, A. Seelig, J. Seelig, and G. Zaccai, Neutron diffraction studies on selectively deuterated phospholipid bilayers, *Nature* **271**, 182 (1978).
94. E. J. Dufourc, C. Mayer, J. Stohrer, G. Althoff, and G. Kothe, Dynamics of phosphate head groups in biomembranes: Comprehensive analysis using phosphorus-31 nuclear magnetic resonance lineshape and relaxation time measurements, *Biophys. J.* **61**, 42 (1992).
95. M. Hong, K. Schmidt-Rohr, and H. Zimmermann, Conformational constraints on the headgroup and sn-2 chain of bilayer DMPC from NMR dipolar couplings, *Biochemistry* **35**, 8335 (1996).
96. H. Hauser, I. Pascher, and S. Sundell, Preferred conformation and dynamics of the glycerol backbone in phospholipids: An NMR and X-ray single-crystal analysis, *Biochemistry* **27**, 9166 (1988).
97. L. M. Strenk, P. W. Westerman, and J. W. Doane, A model of orientational ordering in phosphatidylcholine bilayers based on conformational analysis of the glycerol backbone region, *Biophys. J.* **48**, 765 (1985).
98. M. F. Brown, J. Seelig, and U. Haberlen, Structural dynamics in phospholipid bilayers from deuterium spin-lattice relaxation time measurements, *J. Chem. Phys.* **70**, 5045 (1979).
99. C. Ho and C. D. Stubbs, Hydration at the membrane protein-lipid interface, *Biophys. J.* **63**, 897 (1992).
100. R. E. Jacobs and S. H. White, The nature of the hydrophobic binding of small peptides at the bilayer interface: Implications for the insertion of transbilayer helices, *Biochemistry* **28**, 3421 (1989).
101. M. M. Teeter, Water-protein interactions: Theory and experiment, *Annu. Rev. Biophys. Biophys. Chem.* **20**, 577 (1991).